Classification of Wood with Respect to Strength and Stiffness Using Images and Data of Knot Patterns

Fadia Heimdahl Aldina Pivodic

Autumn 2002

February 18, 2003

Abstract

Knots are of great importance when grading structural softwood. In this master's thesis we investigate 410 beams with respect to their strength and stiffness, given from static bending tests, in relation to the occurrence, size and position of knots. To achieve this we provide a Matlab program, with a Graphical User Interface, which presents different knot measures in relation to predetermined data about the strength and the stiffness of the beams. The obtained knot measures are: knot areas on the face of the beams and the smooth version of them, $TKARF$ and $TKARSF$ respectively, the projected knot areas on the cross-sections and the smooth version of them, $TKAR$ and $TKARS$ respectively, as well as the *fractional* $TKAR$, which is a fractional part of the cross-section of the beam, and the *weighted* $TKAR$, using Moment of Inertia.

The mean value of the results concerning correlation coefficient, R, when correlating the knot measures to the stiffness values is -0.35. The result concerning the strength values, with respect to the failure point, against the $TKAR$ turned out to be -0.38, against the *fractional* $TKAR$ -0.34 and against the *weighted* $TKAR$ -0.43, which in comparison to previous studies can be seen as rather good results. A corresponding examination is done with respect to the centre of the beam instead of the failure point. This examination can be used to predict the strength of the beam, by using linear regression. The result shows the bigger the distance from both sides of the centre point the better correlation to the strength.

The results from this project could be a good start to an automatic grading system in combination with a scanning system.

Acknowledgements

This master's thesis has been carried out at Chalmers University of Technology and Gothenburg University under supervision of Prof. Mats Rudemo whom we would like to thank for all good advises that he has given us, for showing deep commitment and for his encouragement throughout this work.

The project has been done in cooperation with Swedish National Testing and Research Institute in Borås under supervision of MSc Rune Ziethen and PhD Charlotte Bengtsson.

Rune, thank you for being patient with us and for standing by whenever we needed. We would also like to thank you for facilitating our work through your excellent guidance and support.

We would like to give our greatest gratitude to Charlotte Bengtsson and Carl-Johan Johansson, head of section at Wood Materials and Structures, for being there for us and for their valuable advises.

Special thanks to Tomas Ericsson for his good advises concerning Matlab and to Jonas Dahlberg and Tony Heimdahl for helping us with the data files.

Thank you everyone at Wood Materials and Structures for being kind and helpful.

Thank you our friends in master's thesis room for making this period more fun.

I,Fadia, own my parents, sister and brothers grateful gratitude for their understanding and support, and my wonderful husband Tony for being there for me.

I,Aldina, would like to thank my family for their encouragement and their understanding. I am especially grateful to my boyfriend Henrik Ståhlberg. Thank you, Henrik, for all nice words that make me strong and for just being there for me.

Contents

List of Symbols and Abbreviations

$CWAR$	Clear Wood Area Ratio, see Section 2.1
F	Force
G	The Gaussian filter
GUI	Graphical User Interface
h	The height of the beam
I	Moment of Inertia
l	The span of the bended beam
MOE	Modulus of Elasticity
R	The correlation coefficient
SSE	The residual error
$TKAR$	Total Knot Area Ratio, see Section 2.1
$TKARF$	Total Knot Area Ratio Face, see Section 2.1
$TKARL$	Total Knot Area Ratio Lower, see Section 2.1
$TKARS$	Total Knot Area Ratio Smoothed, see Section 2.1
$TKARSF$	Total Knot Area Ratio Smoothed Face, see Section 2.1
$TKARU$	Total Knot Area Ratio Upper, see Section 2.1
w	Deformation of the beam
X, Y	Variables
x_i, y_i	Observed values of the variables X and Y
β_0, $\hat{\beta}_0$	The intercept of a line and its estimated value
β_1, $\hat{\beta}_1$	The slope of a line and its estimated value
μ_{y_i}	The mean value of y_i
ϵ_i	The difference between y_i and μ_{y_i}
σ	The standard deviation

1 Introduction

1.1 Objective of Master's Thesis

The objective of this master's thesis is classification of wood with respect to strength and stiffness using data obtained by image analysis and proof loading machines (a bending type strength grading machines). Wood that is investigated in this work is Norway spruce (*Picea Abies*), originally from a forest, close to Vetlanda in Småland, Sweden.

This project is done in cooperation with Swedish National Testing and Research Institute in Borås. There are saved images and data of 410 beams available. They are obtained by the Soliton Scanning System - a wood scanning system - see Section 2.2. There are also stiffness values available from the Cook-Bolinder Strength Grading machine for the same beams, see Section 2.4, and strength and stiffness values for 198 beams from static bending tests obtained by the Servo-hydraulic Universal Proof Loading machine, see Section 2.5.

A beam can contain several types of defects. We are only examining the knots. Their occurrence, size and location is compared to the stiffness and the strength values of the beam.

This master's thesis provides a Matlab program for projection of the knots on the cross-section of a certain window of the beam. A Graphical User Interface is developed to facilitate the use of the program. All data about knots are taken from the Soliton Scanning System. The projection of the knots gives us an idea about how large part of a beam is covered by knots. This information is, later in the project, correlated to the stiffness values from the Cook-Bolinder Strength Grading machine and the strength values from the Servo-hydraulic Universal Proof Loading machine. We also try to give reasonable answers to the questions below, when we are talking about edgewise bending, see Section 2.3;

1. Are beams symmetric with respect to $TKARU$ and $TKARL$, see Section 2.1?
2. Can we assume that a timber beam is correctly graded even though the ends are not included in the test?

The results presented in this master's thesis could, together with a scanning system, be a good start for an automatic visual grading program.

1.2 Outline of the Report

The first part of the work consists of wood material in general and a review over three studies considering the subject of this master's thesis which can be seen as an introduction for the forthcoming examination. The second section provides the data used in this project. After that the report continue with the theoretical background of this master's thesis, including regression analysis, Gaussian filter and Moment of Inertia.

The algorithms obtained in this master's thesis are outlined in the fourth section together with the results, concerning the stiffness values, of the 15 beams used for the modelling work. Next section handles a comparative study between the algorithms obtained in the fourth section and the strength values.

In the sixth section we give a short explanation of the Graphical User Interface that we have designed for the named algorithms.

Finally, we put together and analyse the results of the 410 beams used in the project and give a conclusion of this master's thesis.

1.3 Background and Literature

1.3.1 Wood Material

The micro-structure of wood, which is built of cells, looks like it is built of small tubes bonded together. The tube width and the wall thickness can vary, but the wall material properties are almost the same in all wood species, with density around 1500 kg/m^3 [9][13], see Figure 1.

A defect in wood is any feature that lowers its value on the market. It may be an abnormality that decreases the strength of the wood or a characteristic that limits its use for a particular purpose. Many defects are not abnormalities in a strict sense, but are simply the product of natural growth. Knots and reaction wood are such natural defects. Other natural defects are those created by the external environmental factors, such as wind, heavy snow, severe cold, heat or lightning. For instance compression wood, tension wood, top rupture, slope of grain are other the most common natural defects [9].

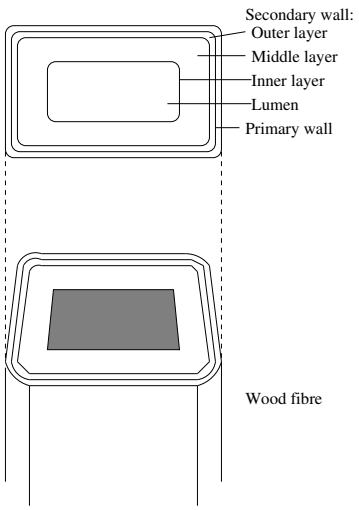

Figure 1: The micro-structure of wood

Knots

A knot is a branch that is embedded in the main stem of a tree and it is the most common and influential defect. For Norway Spruce, a softwood used for structural purposes, the branches occur as whorls at more or less regular intervals producing knot clusters [8].

The knots causes a disturbace so that the grain angle deviates from zero (parallel to grain). The reduction in strength is caused by the tension that knots produce in perpendicular direction to the grain [13]. This direction is the weakest direction in wood. The stiffness, normally expressed as MOE (Modulus Of Elasticity) which is a good predictor of the strength, is also affected by the fibre distortion. MOE contains information about the clear wood properties and beside that also information about different defects such as knots, slope of grain etc.

Both the location and the size of the knots affect the strength of a beam. For instance knots which are located near the edge of a beam, in tangential direction, see Figure 2, are of particular importance. A bigger knot then usually reduces the strength more than a smaller knot [4].

The sawing pattern and location of a beam in the log influence how the knots affect the strength. There are two different methods to saw a log commonly used today. Using both methods the log is first cut as a parallelepiped. Then the log is cut again using either 2x-log or 3x-log method.

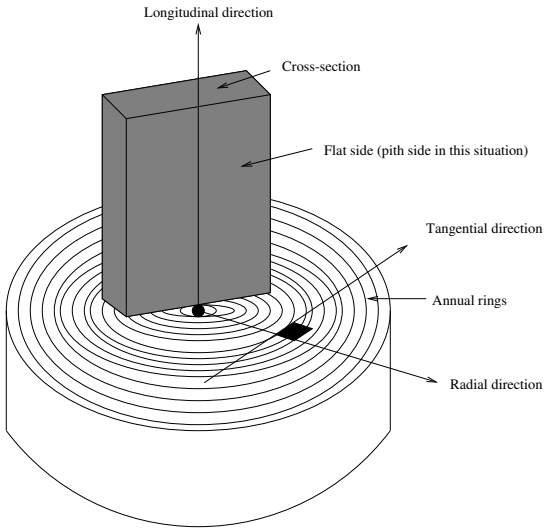

Figure 2: Definition of the geometrical parameters

For logs with larger diameter other methods can be used, for instance 4x-log. 2x-log method cuts the log in two pieces so that the pith appears on the flat sides of the beams. 3x-log method cuts the log in three pieces. The pith appears inside the middle beam. Depending on which method that is used we get three different cases for the pith position. They are: in the middle of the beam, on its flat side or outside the beam. This is necessary information when assessing the appearance of the knots.

Depending on the knots position in the log, we get different kinds of knots on the beams when sawing, for example sound knots, dry knots and decay knots. In this master's thesis we treat all knots alike. The appearance of a knot in a beam depends upon the direction of cut through the included branch. When the cut is made along the axis of the branch, the knot appears as a spike knot on the surface of the beam. When a transverse cut is made through the branch, the knot appears round or oval.

1.3.2 Previous Work

Modelling the Variability of Bending Strength in Structural Timber - by Tord Isaksson [6]

A part of Tord Isaksson's doctoral thesis provides a theoretical version of our master's thesis. Isaksson proved that the projected knot area on the cross-section can, especially in combination with some other data, for instance MOE, in the highest degree give an estimation of the strength of the beam. Bending and tensile strength are in this report related to Clear Wood Area Ratio ($CWAR = 1 - TKAR$), Cook-Bolinder values, Finnograder values and some combination of these. The best result considering bending strength, that the experiments gave, was a combination of MOE on the flat side, see Figure 2, with the ratio between the biggest knot diameter on the tension edge and the width of the beam. When Isaksson included the distance from the flat side of the beam to the centre of the knot on the edge, it seemed to give very little new information. On the other hand using only knots as related data, as is done in this master's thesis, Isaksson shows that knots on the flat sides nearer to the edges than to the centre are of bigger influence.

Grading of Timber with Respect to Mechanical Properties - by Carl-Johan Johansson [8]

This article, as well as Isaksson's doctoral thesis, covers mostly the relations between different measures, different knot data and bending or tensile strength. It mentions that knots alone are poor predictors of strength. But taking the size (Kunesh et al. (1972)), position (Schniewind et al. (1971) and Johansson (1976)), or vicinity from the edges, into account, the correlation to the tensile strength can be increased. The presence and the size of the knots is one reason to that the relation between the bending strength and MOE differs from one location to another. This article note also that adding the edge knot data to the flatwise MOE improves the bending strength prediction considerably (Boström (1998)).

Automatic Inspection of Sawn Wood - by Erik Åstrand [1]

Åstrand's doctoral thesis covers mainly two different problems concerning automatic inspection of sawn wood. Firstly it brings up the problem of detecting defects on wood surface. Secondly it brings up the process of optimizing the cutting process, when boards are cut into products, based on the information when detecting defects. A knot is generally the most common defect on a beam. Some other defects are splits, pitch pockets, pith stripes,

bark pockets, blue stain, decay and compression wood. Most of these defects have a characteristic shape or darkness and therefore Åstrand can easily detect them on a gray-scale image. Other defects, however, like blue stain, decay and compression wood requires according to Åstrand additional spectral information or textural methods to be detected. After identifying the two problems, mentioned above, Åstrand formulates two objectives. Firstly, he sets out to develop new image processing methods and algorithms for wood defect detection. And, secondly, he sets out to optimize the utilization of wood material by using the defect information. Åstrand has achieved high-speed image processing using integrated sensors, so called smart sensors, or smart cameras, where low-level image processing takes place directly on the sensor chip, for more information see [2]. He has also developed the traditional method for measuring tracheid effect, see Section 2.2, by using smart image sensors. This method is nowadays used in the Soliton Scanning System.

2 Available Data

2.1 Test Material

The test material included in this master's thesis consists of 410 beams which are currently located at Swedish National Testing and Research Institute in Borås. They are of size $145 \times 45 \times length\ mm^3$. The *length* varies from 2800 *mm* to 4600 *mm*. All 410 beams are tested in the Cook-Bolinder Strength Grading machine, flatwise bending, see Section 2.3, which gives an output of force values that are proportional to the stiffness of the beams, see Section 2.4. These values are designated as stiffness values through out this master's thisis. 198 beams are tested in edgewise bending, see Section 2.3, using the Servo-hydraulic Universal Proof Loading machine, where both strength and stiffness values are available outputs. Concerning the last named bending tests we are only using the strength values.

All the beams are run through the Soliton Scanning System. Beam images and data files, data matrices, obtained by the system are used when providing the Matlab program. In the program the beams are examined in different *windows*, see Figure 3, default value 140 *mm*, for every 10 *mm movement* to be able to compare the results to the Cook-Bolinder, stiffness, values where the examination of the beams is done using the same procedure.

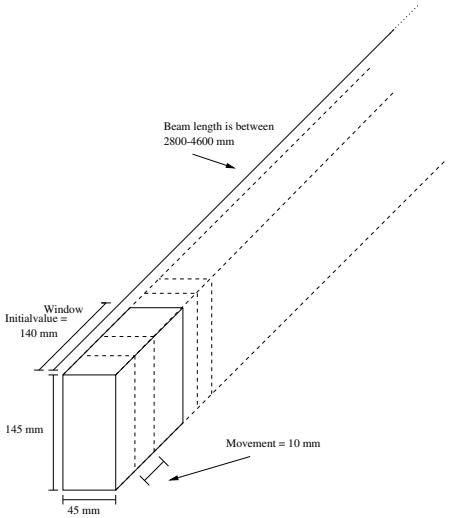

Figure 3: Typical beam dimensions, with *window* and *movement*

We have chosen to work with 15 beams as a starting point for developing the algorithms and the mathematical model.

The following knot measures obtained from the cross-section of a beam, some of them illustrated in Figure 4, are worth explaining before coming into the problem solving:

1. $CWAR$, *Clear Wood Area Ratio*, is the fraction between the total clear wood, non-knotty, area on the cross-section of the window and the area of the cross-section, can even be explained as $1 - TKAR$
2. $TKAR$, *Total Knot Area Ratio*, is the fraction between the total knot area on the cross-section of the window and the area of the cross-section
3. $TKARF$, *Total Knot Area Ratio Face*, is the ratio between the total knot area on the window face and the total area of the window
4. $TKARL$, *Total Knot Area Ratio Lower*, is the fraction between the total knot area of the lower part of the cross-section of the window and the part of the area of the cross-section
5. $TKARS$, *Total knot Area Ratio Smoothed*, is the smoothed $TKAR$, see Section 3.2
6. $TKARSF$, *Total Knot Area Ratio Smoothed Face*, is the smoothed $TKARF$, see Section 3.2
7. $TKARU$, *Total Knot Area Ratio Upper*, is the fraction between the total knot area of the upper part of the cross-section of the window and the part of the area of the cross-section

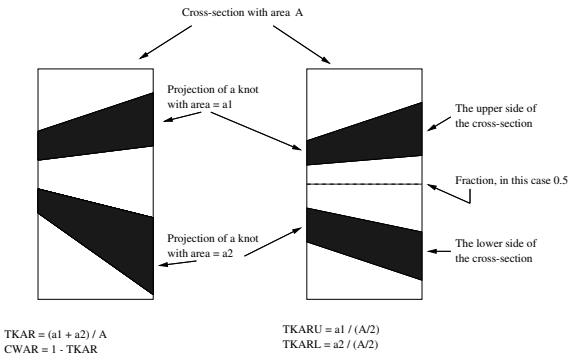

Figure 4: The definitions of the knot measures

2.2 Images and Output from the Soliton Scanning System

The Soliton Scanning System is used to detect defects on wood surface by using the tracheid effect, see *The Tracheid Effect* below. The system contains 4 multi-sensor cameras, 6 line lasers and a standard PC [17].

It scans, does different measurements on the piece of wood and presents the results such as images and statistics that can be analysed or saved for future work. The defects can be discerned by different colours on the images. Figure 5 and Figure 6 show the output from the Soliton Scanning System.

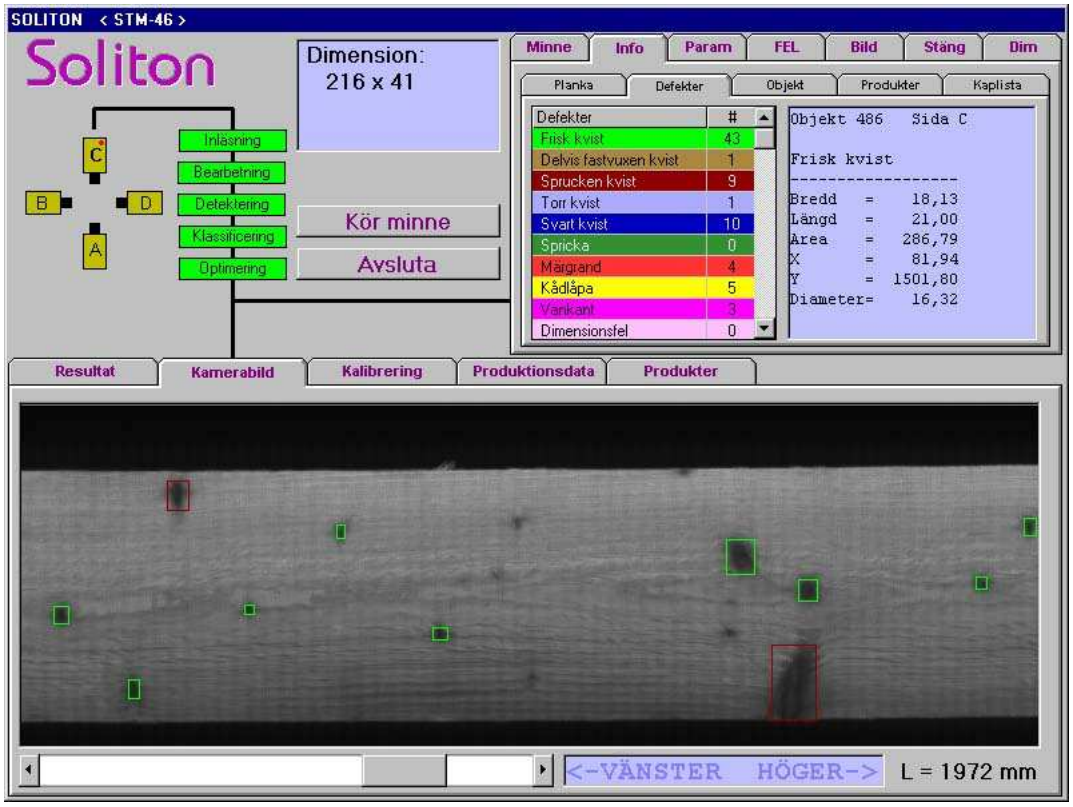

Figure 5: The output from the Soliton Scanning System

From the Soliton Scanning System the following data are used in this master's thesis:

1. Type of the defect
2. Position of the defect
3. Length, width and area of the defect

The only defects that are studied in this master's thesis are knots which are visualised on the images from the Soliton Scanning System. These images are used in different visual comparisons through out the project.

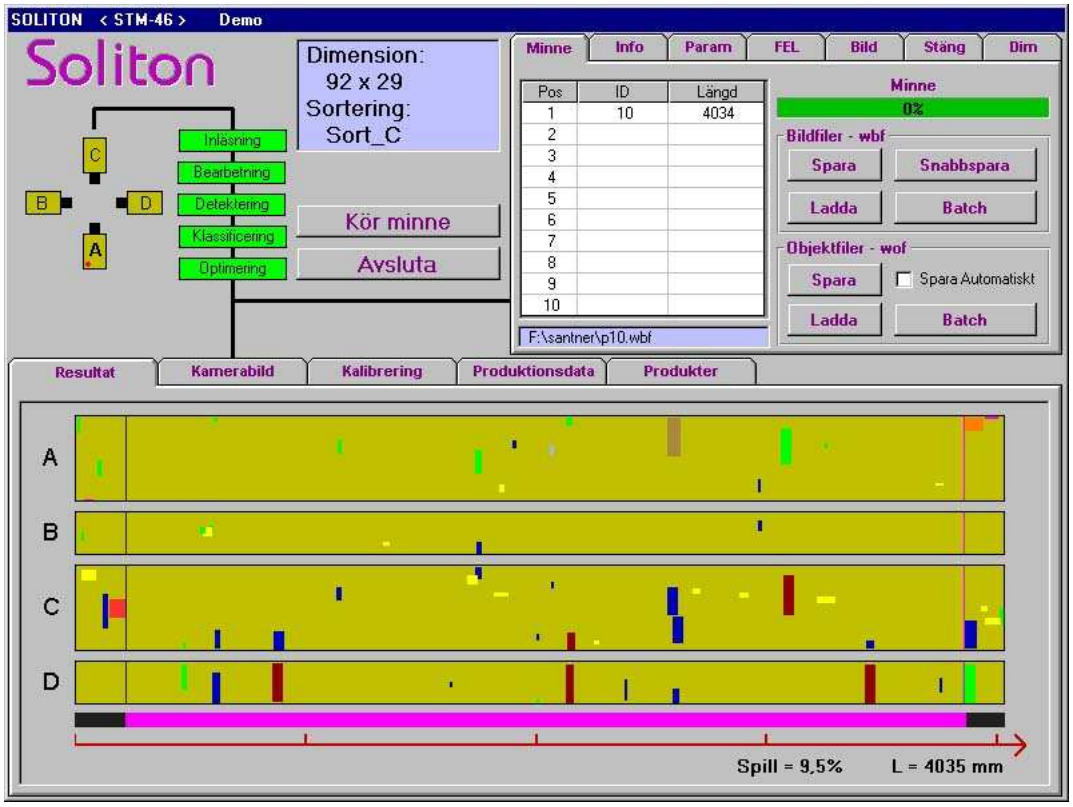

Figure 6: The output from the Soliton Scanning System

The Tracheid Effect

The word *tracheid* originate from the *tracheids* which are the fibres in soft-wood. The tracheid effect is the spread of light in the wood surface [8][11]. The amount of light spreading is dependent on the density. For denser parts of wood, for instance a knot, the spread of light is less. This method helps to easily detect bright knots, which are visually hard to discern. By using the tracheid method the density of wood can roughly be estimated.

The system for tracheid effect scanning consists of a GPC-camera, based on MAPP2200 smart image sensors [2], and a diode laser with line generating optics. The laser illuminates a thin line on the wood surface, while the sensor measures the intensity on both sides near the line, but not on it [11]. To achieve this effect it is necessary for the optical plane of one line of the sensor array of the camera and the plane of light of the laser to coincide, see Figure

7.

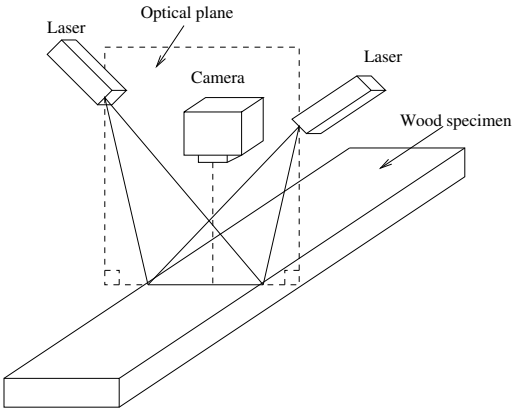

Figure 7: Wood inspection system

2.3 Two Types of Bending

Bending of beams can be done in two different directions, flatwise and edgewise. Figure 8 shows the difference between these two. The Cook-Bolinder Strength Grading machine, see Section 2.4, bends the beam in flatwise direction to obtain stiffness values, while the Servo-hydraulic Universal Proof Loading machine, see Section 2.5, uses edgewise bending principle to obtain strength and stiffness values.

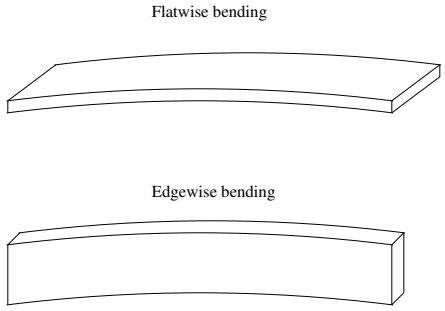

Figure 8: Flatwise and edgewise bending

2.4 The Cook-Bolinder Strength Grading Machine

The Cook-Bolinder Strength Grading machine, see Figure 9, measures the force required to cause a certain pre-set flatwise deflection of the beam over a span of 900 mm [6]. In our case, the pre-set deflection is 5.9 mm because it depends on the thickness of the beam which is 45 mm. The beam runs through the machine at a speed of 48 m/min and force is recorded every 10 mm along the beam, excluding 450 mm at both ends. The beam runs through the machine in two opposite loading directions, and the average flatwise stiffness of the two results is taken to eliminate the initial bow of the beam.

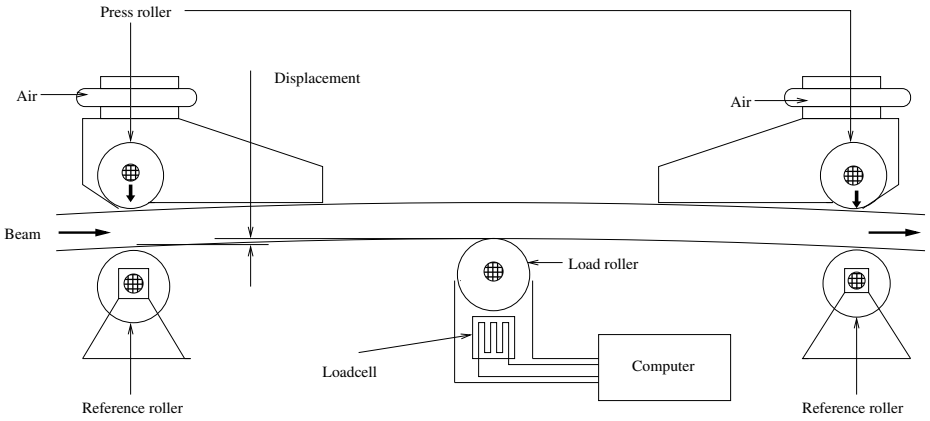

Figure 9: The Cook-Bolinder Strength Grading machine

The flatwise MOE can be calculated from the measured force, F, and prescribed deflection, w,

$$MOE = \frac{Fl^3}{48Iw}$$

I is the Moment of Inertia, see Section 3.3 and l is the span.

Typical results from the Cook-Bolinder Strength Grading machine from one of the beams used in this project, here beam number 370, are shown in Figure 10 below. Cook-Bolinder values are in fact the force values named above, which are proportional to the stiffness values.

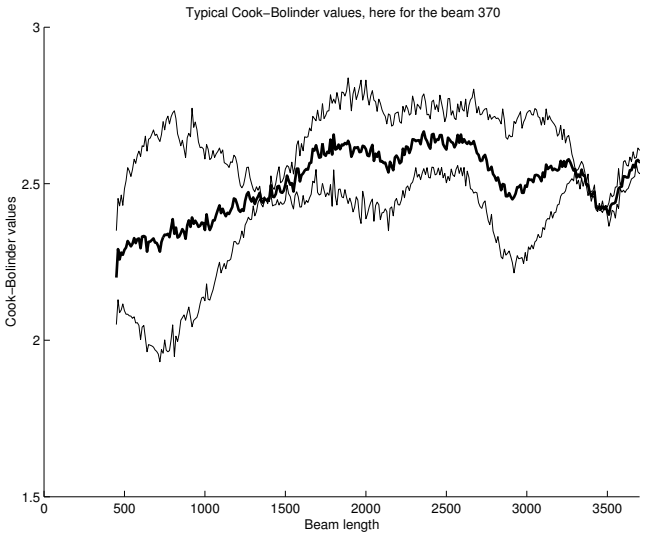

Figure 10: Typical results, force values, from the Cook-Bolinder Strength Grading machine, here for the beam number 370. The bold curve is the average stiffness values.

2.5 Servo-hydraulic Universal Proof Loading Machine

Servo-hydraulic Universal Proof Loading machine is used to carry out the edgewise bending of the beams to determine bending strength and stiffness according to the European standard EN 408 (four-point loading) with a span-to-depth of 18 [16]. The loading capacity of this machine is 100 kN.

The first step of the procedure is to predict the break section, usually where the biggest knot is located. The predicted section is then placed in the centre of the proof area of the machine between the loads, see Figure 11. According to the European standard measures this area should be of $6h$, where h is the height of the beam. The loads are incremented several times until the beam is broken. The modulus of elasticity is obtained according to the equation below [15]:

$$MOE = \frac{6hl^2(F_2 - F_1)}{16I(w_2 - w_1)}$$

where
l is the tested section, equal to $5h$

$F_2 - F_1$ is the increment of load, measured in N
$w_2 - w_1$ is the increment of deformation corresponding to $F_2 - F_1$, measured in mm
I is the Moment of Inertia, measured in mm^4

The bending strength f is given by the equation:

$$f = \frac{Fl}{bh^2}$$

where b is the width of the beam.

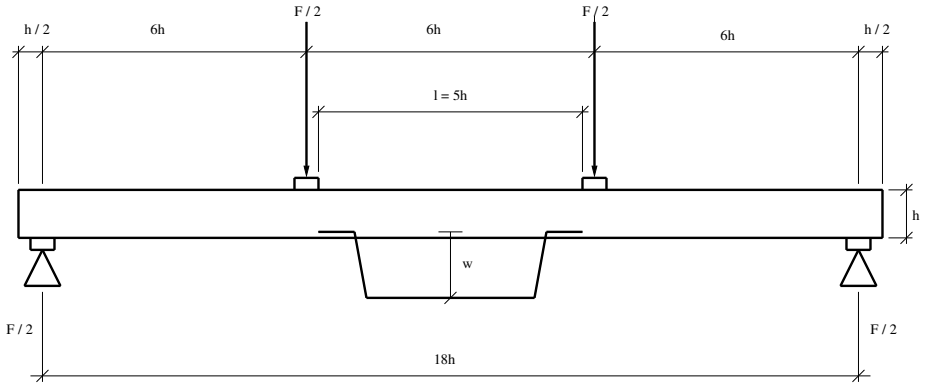

Figure 11: Schematic figure of the Servo-hydraulic Universal Proof Loading machine

3 Theory

3.1 Regression Analysis

Let X be a variable and Y be a random variable. The collection of n pairs (x_i, y_i), where x_i is an observed value of the variable X and y_i the corresponding observation for the random variable Y, is the data we are working with. More directly, it means that x_i is the ratio between the projected areas of the knots on the cross-section of a certain window and the corresponding total window area, while y_i is the Cook-Bolinder value for the beam in the same window.

In order to fit a line to a group of data points we need to estimate the parameters in the equation for a straight line

$$y = \beta_0 + \beta_1 x$$

This is the idea behind the *Simple Linear Regression* model, which can be expressed as below [10],

$$y_i = \beta_0 + \beta_1 x_i + \epsilon_i$$

y_i are random variables for $i = 1...n$. β_0 denotes the intercept and β_1 the slope of the regression line. ϵ_i denotes difference between every y_i and its mean value μ_{y_i}. x_i and y_i are given variables while β_0 and β_1 need to be estimated. That is easily done by using the *Least Square Method*, which sets the best fit line to be the one that has the least sum of squares of the residual errors e_i, denoted by SSE. Residual error is the sum of squared deviations.

$$SSE = \sum_{i=1}^{n} e_i^2 = \sum_{i=1}^{n} (y_i - \hat{\beta}_0 - \hat{\beta}_1 x_i)^2$$

$\hat{\beta}_0$ and $\hat{\beta}_1$ are the estimated values of β_0 and β_1 respectively. The equations for them are:

$$\hat{\beta}_1 = \frac{n \sum_{i=1}^{n} x_i y_i - (\sum_{i=1}^{n} x_i)(\sum_{i=1}^{n} y_i)}{n \sum_{i=1}^{n} x_i^2 - (\sum_{i=1}^{n} x_i)^2}$$

$$\hat{\beta}_0 = \frac{1}{n} \sum_{i=1}^{n} y_i - \hat{\beta}_1 \frac{1}{n} \sum_{i=1}^{n} x_i$$

The sample correlation coefficient R is estimated as below:

$$R = \frac{n\sum_{i=1}^{n} x_i y_i - (\sum_{i=1}^{n} x_i)(\sum_{i=1}^{n} y_i)}{\sqrt{n\sum_{i=1}^{n} x_i^2 - (\sum_{i=1}^{n} x_i)^2}\sqrt{n\sum_{i=1}^{n} y_i^2 - (\sum_{i=1}^{n} y_i)^2}}$$

3.2 Gaussian Filter

Filters in general are used to affect an image or a signal in a certain way, for instance in order to smooth image or the signal or detect the edges in the image [5]. A function f_1 can be affected by a filter G in either frequency or time domain.

1. Frequency domain: $F_2 = GF_1$, where F_1 is Fourier transform of f_1 and F_2 Fourier transform of f_2 and where

   $$f_2(x) = \sum_{y=1}^{n} G(y)F_1(y)e^{i2xy\pi}$$

   is the function of interest.

2. Time domain:

   $$f_2(y) = H * f_1 = \sum_{x=1}^{n} f_1(x)H(y-x)$$

   where $*$ denotes convolution and H is the Fourier transform of G.

The data that we would like to affect looks, in general, like the non-smoothed curve in the lower part of Figure 13.

A standard Gaussian filter can be used to smooth this kind of curves [14]. It is denoted by $G(x)$. The Fourier transform of G is the same function, which gives $G = H$. $G(x)$ is denoted by:

$$G(x) = e^{-\frac{x^2}{2\sigma^2}}$$

or with a normalising factor

$$G(x) = \frac{1}{\sigma\sqrt{2\pi}}e^{-\frac{x^2}{2\sigma^2}}$$

The standard deviation σ is the only parameter of the Gaussian filter. It is proportional to the size of the neighbourhood on which the filter operates. Values more distant from the centre of the operator have smaller influence.

By doing a sensitivity analysis the most optimal value of σ can be chosen which gives the best result for all data together. The optimal σ for the projected knot areas is decided by first calculating the optimum for each beam following by taking the mean value of the optimum of all beams.

The smoothing process is obtained using the algorithm described below:

1. Set the Gaussian filter $G(x)$ to be a vector of size $2\sigma + 1$
2. Convolve data $f(x)$ with the filter $G(x)$

$$f * G = \sum_{i=1}^{n} f(i)G(x - i)$$

where f is a vector of length n.

3.3 Moment of Inertia

The Moment of Inertia of areas, also called *The Second Moment*, is the product of each area element included in a area section, A, and the square of its distance, y, from a specific axis [3]. The sum of all these products gives the Moment of Inertia of the area section A. The mathematical formulation of the Moment of Inertia with respect to the x-axis and the y-axis is:

$$I_x = k \int y^2 dA$$

$$I_y = k \int x^2 dA$$

The Parallel-axis Theorem (Steiner Theorem)
The Moment of Inertia I of an area A with respect to any given axis is equal to the Moment of Inertia $\bar{I}$ of the area with respect to a centroidal axis (the axis through the centroid C of the area) parallel to the given axis, plus the product of the area A and the square of the distance d between the two axes. This theorem can be formulated as following [3]:

$$I = \bar{I} + Ad^2$$

Example: The Moment of Inertia of a Rectangular Area
The Moment of Inertia of a rectangle with respect to its base can be determined by first dividing the rectangle into strips parallel to the x-axis,

$$dA = bdy$$

$$dI_x = y^2 bdy$$

$$I_x = \int_0^h by^2 dy = \frac{1}{3}bh^3$$

The I_y is determined in the same way. The Parallel-axis theorem applied on the rectangle in Figure 12 gives the Moment of Inertia:

$$\bar{I}_{\acute{x}} = \frac{1}{12}bh^3$$

$$I_x = \bar{I}_{\acute{x}} + Ad^2 = \frac{1}{12}bh^3 + bh(\frac{h}{2})^2 = \frac{1}{3}bh^3$$

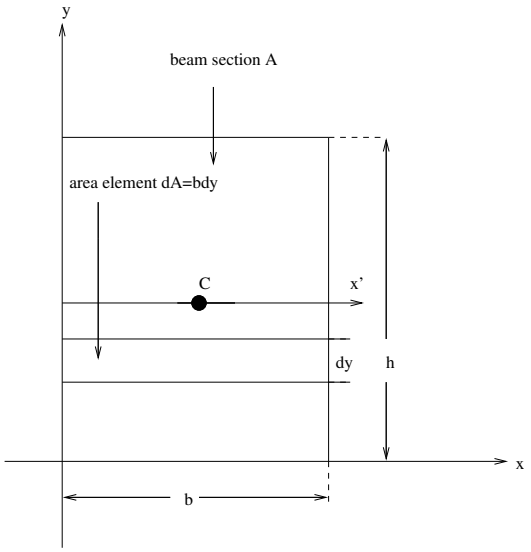

Figure 12: Moment of Inertia of a rectangular area

4 Analysis of Images / Projected Area

4.1 Specification of the Subject

The objective is to find the relation between the occurrence of knots and the stiffness of a beam. The found relation should be valid for every 10 mm of the beam.

The following variables should be included in the function:

1. The location of the pith

   We have three different cases: the pith outside the beam, the pith on the beam and the pith inside the beam. This information is decided by visual observation of the beams.

2. The window width, default value 140 mm

   We are starting to examine the first 140 mm of the beam. Using that window we will estimate the projected area of the knots on the cross-section using data about defects, given from the Soliton Scanning System.

3. The movement of each estimation of the knot area , default 10 mm

   The same procedure as in the previous point will be done every 10 mm.

4. The part of the cross-section that will be estimated, default 0.25

   A comparison between the projected knot area which is located in $0 - 50\%$ of each end of the cross-section should be done to find out if difference in the projected knot area ($TKAR$) and the strength exists.

5. Weight function of knot area depending on the position of the knots

   This is of importance because the knots which are located near the edges influence the strength more than the others, when bending the beam in edgewise direction with the Servo-hydraulic Universal Proof Loading machine.

The result should be presented in a text file including positions and different knot measures.

To meet the objective we use data from the Soliton Scanning System and data from the Cook-Bolinder Strength Grading machine and correlate them to each other to find relation between the stiffness of the beam and its knot

measures. The same procedure is done with the strength values from the Servo-hydraulic Universal Proof Loading machine. The statistical method that we are going to use here is linear regression.

4.2 Examination of the Face Knot Area in a Window

To convince ourselves about the relation between the knots and the stiffness of a beam we start with an easier problem. The problem is to calculate the ratio value between the face knot area of the knots in a window and a window area and compare it to the stiffness values of the same beam. We examine data from 15 different beams. We use a window size of 140 mm with 10 mm movement along the flat side of the beam. The ratio value, $TKARF$, from every window is plotted along the beam against the stiffness values. We can see that when the knot area is big, the Cook-Bolinder curve decreases, see Figure 13. From the plot of the Cook-Bolinder curve we can also see that the knots affect a certain area around them. To get a better comparison between face knot area and Cook-Bolinder curve, we take into consideration a certain area around the knots, σ, which results in the smoother curve of the knot area, $TKARSF$ in Figure 13. The smoothing algorithm is described in Section 3.2.

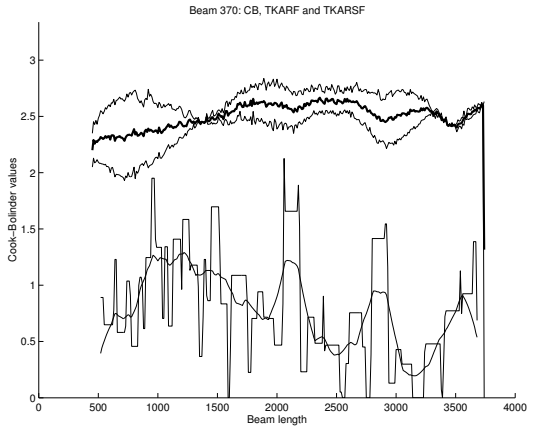

Figure 13: $TKARF$, the unsmoothed curve in the lower part of the figure, $TKARSF$, the smoothed curve in the lower part of the figure, and Cook-Bolinder values, the upper part of the figure, along the beam number 370.

We also plot the Cook-Bolinder values against the face knot area, $TKARF$.

Using *Least Square Method*, see Section 3.1, in Matlab we can fit a line to the plotted values. In most cases, as expected, the line decreases as the area of the knots increases, see Figure 14. In a few cases, however, the opposite occurs. This can be explained with occurrence of other defects on the beam which affect the stiffness. For the beam 370 we get a correlation coefficient, R, of -0.2633. Using the smoother curve of the knot area, $TKARSF$, the correlation coefficient increases to -0.3506.

The maximum value on the x-axis is set to be the maximum of $TKARF$ and $TKARSF$ to get better comparison among the figures. This is the case in all figures where we fit a line to the data.

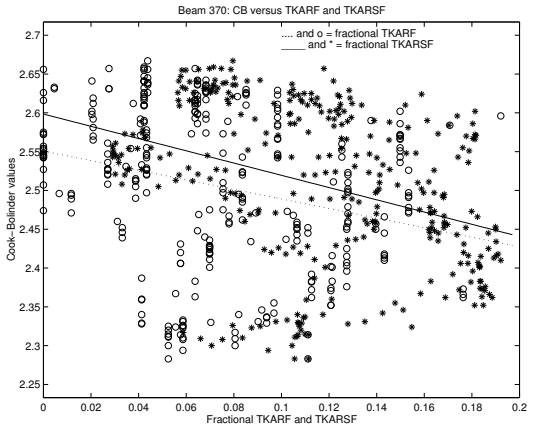

Figure 14: Stiffness against $TKARF$ with fitted line and stiffness against $TKARSF$ with fitted line for the beam 370.

4.3 Projection of the Knot Area in the Cross-Section of a Window

4.3.1 Algorithm - Find-a-partner

This algorithm is built for the beams that have the pith outside, which means that the knots come through one side, in-come side, and go out on one of the other three sides, out-come sides. The algorithm *Find-a-partner* finds the corresponding knot on one of the out-come sides for one knot on the in-come side. The in-come side is determined using the number of knots on each flat side. Observations on the beams show that the number of knots is larger

on the in-come side of the beam. The following restrictions to find the right partner are included in the algorithm:

1. The partner shall not be located on the in-come side of the beam.
2. The partner is located on a fix distance from the knot in the longitudinal direction of the beam. See the lower part of Figure 15.
3. If the in-come side is side 0:
   (a) The knots located on the upper third part of the in-come side go out either on the edge side number 3 or the lower 2/3 part of the flat side number 2. See the upper left part of Figure 15.
   (b) The knots located on the lower third part of the in-come side go out either on the edge side number 1 or the upper 2/3 part of the flat side number 2. See the upper left part of Figure 15.
4. If the in-come side is side 2:
   (a) The knots located on the upper third part of the in-come side go out either on the edge side number 1 or the lower 2/3 part of the flat side number 0. See the upper right part of Figure 15.
   (b) The knots located on the lower third part of the in-come side go out either on the edge side number 3 or the upper 2/3 part of the flat side number 0. See the upper right part of Figure 15.
5. Knots located in the middle, 1/3 part in the middle of the in-come side, are allowed to go out only on the flat sides.
6. If there are more than one possible partner, choose the nearest one on the longitudinal direction.

The result of this algorithm can be seen in Figure 21 and Figure 22. As shown in the figure, all knots do not have a partner on the out-come side. There are different reasons why this problem occur and one of them is that the Soliton Scanning System does not detect all knots especially if the knots are very small. The restrictions above are another reason. They also cause several other problems, for instance some of the knots choose the same partner. Another problem appears when the partner is located on the edge and hence belongs to two sides of the beam. The algorithm chooses only one of these. These problems proved to be of less importance due to the comparison of the results with the calculations made by visual inspection of 15 beams.

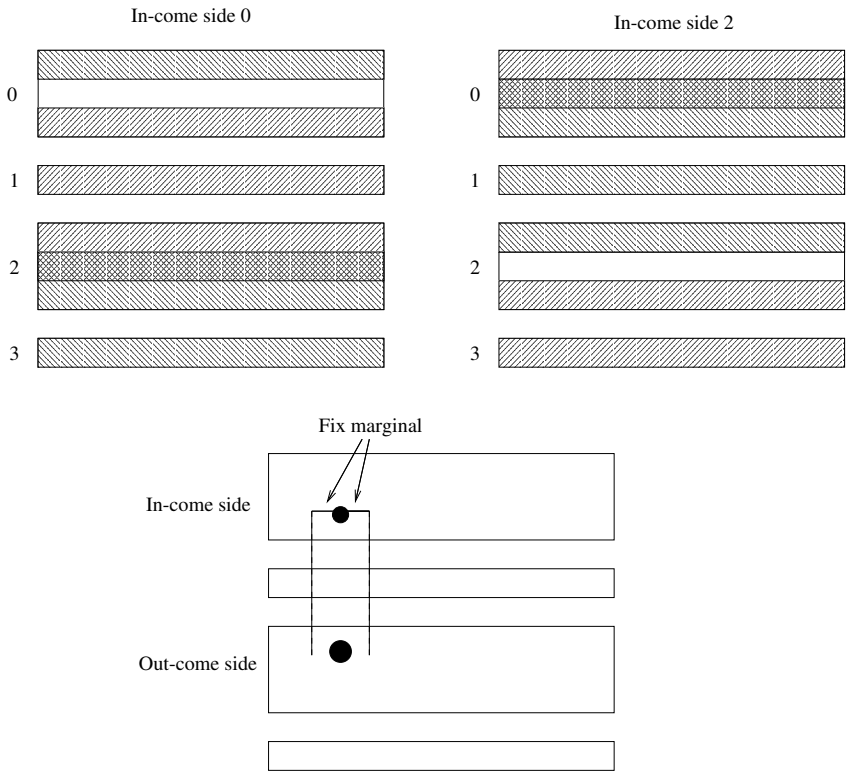

Figure 15: Some of the restrictions of the algorithm Find-a-partner

4.3.2 Projection Algorithms

The projection of the knot areas on a cross section is found using two different methods, *Projection I* and *Projection II*. Both methods are based on geometrical calculations. Calculations of the first one only use the positions of the knots as a starting point. In the second the calculations are obtained using the positions of the knots and image processing. In both cases, the problem is divided into three starting points, depending on the location of the pith.

The three starting points are:

1. The pith is outside the beam.
2. The pith is on the flat side of the beam.
3. The pith is in the middle of the beam.

Figure 16 below describes the projection areas of the knots, on the cross-section. The problem of overlapping knots can occur in several cases in a window, for instance if knots are located in the same tangential direction, see Figure 2, or when detecting one knot as few knots because of the differences in its gray-scale, see Figure 17. In this project we choose to disregard these problems.

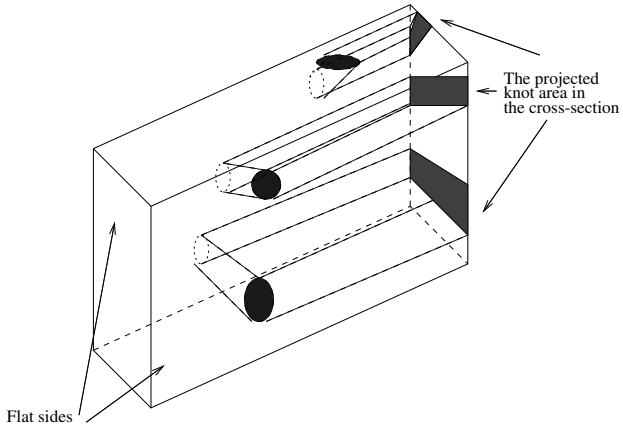

Figure 16: A window with the projected knot areas of a beam

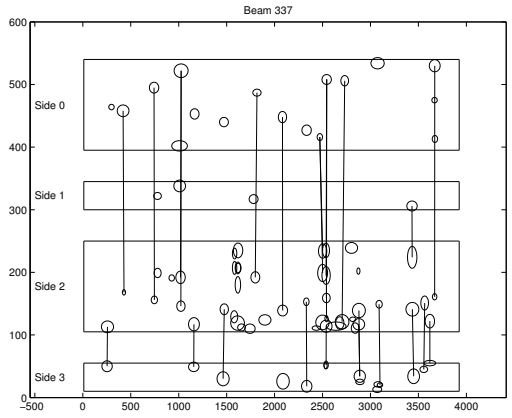

Figure 17: The appearance of the beam 337, with several overlapings. *fractional* $TKAR$, which is a fractional part of the cross-section of the beam.

Projection I

Concerning the first method of calculating the projection, the projected area on the cross-section, $TKAR$, is obtained by calculating the area of the trapeze made by the knot and the corresponding partner, see Figure 18 which shows the appearance, in general, of projected knot area on a cross-section.

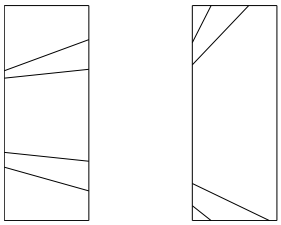

Figure 18: Different possibilities for the projected knot area on the cross-section with the pith outside the beam.

When the pith is on the beam or in the middle of it, the knots don't have a corresponding partner and therefor the *Find-a-partner* algorithm is not needed. Here, the area of a triangle is calculated instead of the trapeze to get the projected area, see Figure 19.

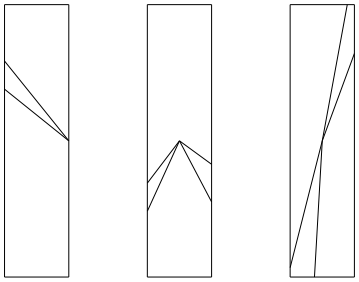

Figure 19: Different possibilities for the projected knot area on the cross-section. The first picture concerns the pith on the flat side, and the others when the pith is inside the beam.

Projection II

This algorithm is based on image processing. The idea is to count the number of pixels which belong to the projected area of the knots. An image is plotted for every window which makes Projection II more realistic and trustful than Projection I, see Figure 20. The image size is proportional to the cross-section dimensions and by choosing larger image size, the calculations get better. We have chosen an image size that optimizes good results together with a fast algorithm.

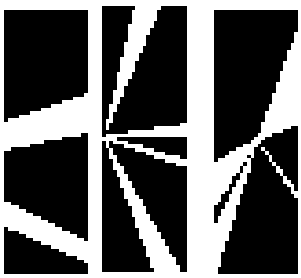

Figure 20: The resulting images from random windows of the Projection II algorithm. The first is from beam 363 which has the pith outside, the second from beam 150 with the pith on it and the third from beam 179 with the pith inside.

As in Projection I, this algorithm is based on the three starting points named above. To satisfy the fourth variable in Section 4.1 a new feature is introduced. The cross-section is divided into upper and lower part, which

results in $TKARU$ and $TKARL$. The size, $0 - 50\%$ of these parts, is an input variable in the algorithm. If the variable is chosen to be 50%, the observed part of the cross-section is then equal to the total cross-section area.

In all three starting points the equation of a straight line is used to define the region that belongs to the projected knot area. The pixels that belongs to this region are then set to one and the rest of the matrix remains zero. The fraction between the sum of all ones in upper/lower part and the area of the corresponding part of the cross-section in each window is an estimation of the projected knot area for the upper/lower part ($TKARU/TKARL$).

4.4 Stiffness Versus Projection Values for the 15 Beams

The correlation between the stiffness values and the knot measures for the 15 beams are obtained using the algorithms described above. They can be seen in Table 1 in the end of this section.

We have chosen to illustrate results of four beams, beams 363 and 364 with the pith outside, beam 370 with the pith on the flatside and beam 179 with the pith inside. These beams are representative for the group of 15 beams that we have tested.

In Figure 21 and Figure 22 the result of the algorithm *Find-a-partner* together with the appearance of the beams 363 and 364 can be seen. We can see from the figures that beam 363 has side 2 as the in-come side, as that the knots are paired to the knots on the other three sides. We can also see several of the problems that we already have mentioned above. For instance, we have the problem when two knots choose the same partner and also when some knots remain without partner. On the other hand, beam 364 is almost perfect. It is worth mentioning that these two beams are rather easy to work with for the reason that they do not consist of many knots that are clustering.

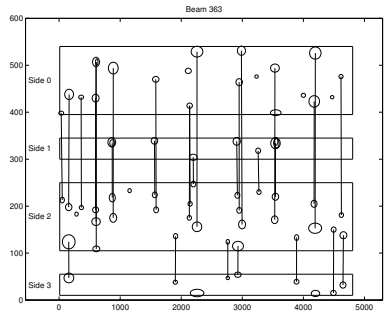

Figure 21: The knots and their corresponding partners on the out-come sides for the beam 363. The pith for this beam is located outside. The in-come side for beam 363 is 2.

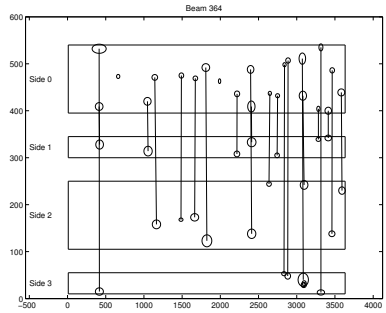

Figure 22: The knots and their corresponding partners on the out-come sides for the beam 364. The pith for this beam is located outside. The in-come side for beam 364 is 0.

The appearance of the beams 370 and 179 can be seen in Figure 23 and Figure 24. In these cases we do not need to find the corresponding knots because the fact that the knots always grow from the pith and the pith is located on, or inside, the beam.

The both algorithms for projection have been implemented for the 15 beams. The differences in the results are at most $10 - 15$ percentage points. The following results, and the results through out this report, are obtained by using Projection II algorithm. As we mentioned before in this algorithm we are able to follow every step of the calculations which makes it easier to control its correctness. Another important advantage is that by using Projection II we are able to satisfy the fourth variable in Section 4.1.

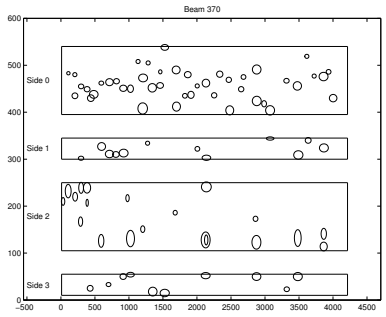

Figure 23: The appearance of the four sides of the beam 370

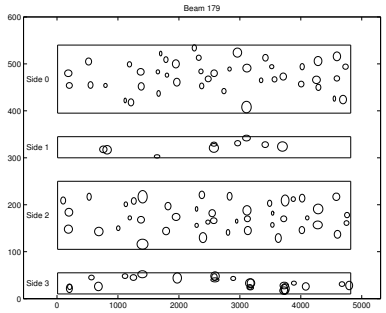

Figure 24: The appearance of the four sides of the beam 179

The results of the projection algorithm, $TKAR$, the smooth projection, $TKARS$, and their relation to the Cook-Bolinder values are shown in Figure 25, for beam 363, Figure 26 for beam 364, Figure 27 for beam 370 and Figure 28 for beam 179. In these figures we also plot Clear Wood Area Ratio , $CWAR = 1 - TKAR$, which can be seen as a prediction to the stiffness values. This curve is very hard to discern in Figure 25 and Figure 26 because it follows the mean curve of MOE very good, while in Figure 27 and Figure 28 we can see a thin curve that is trying to follow the mean MOE as good as possible. More detailed plots, including $TKARF$ and $TKARSF$, are shown in Appendix A.

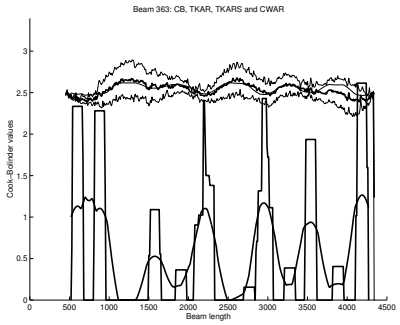

Figure 25: Relation between the Cook-Bolinder values, $TKAR$, $TKARS$ and $CWAR$ for the beam 363.

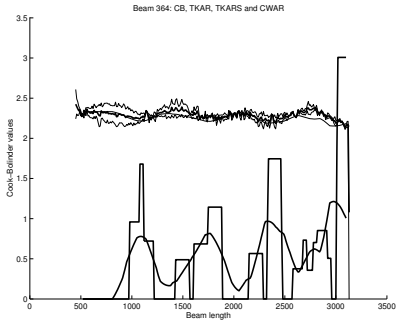

Figure 26: Relation between the Cook-Bolinder values, $TKAR$, $TKARS$ and $CWAR$ for the beam 364.

The plotted values of stiffness against the face knot area, $TKARF$, together with the projected knot area, $TKAR$, and smooth face knot area, $TKARSF$, together with the projected knot area, $TKARS$, and their linear relations for the beams named above are shown in Appendix A.

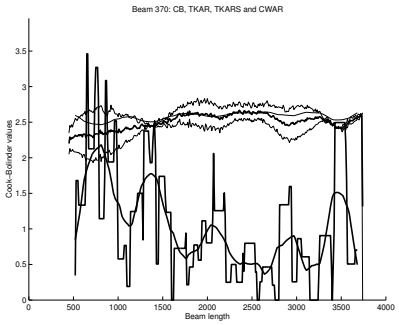

Figure 27: Relation between the Cook-Bolinder values, $TKAR$, $TKARS$ and $CWAR$ for the beam 370.

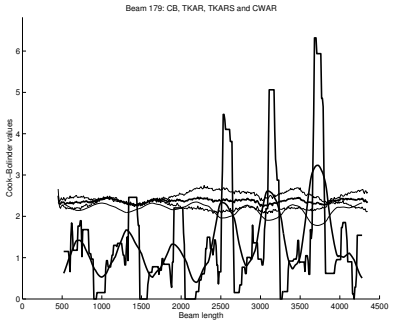

Figure 28: Relation between the Cook-Bolinder values, $TKAR$, $TKARS$ and $CWAR$ for the beam 179.

The correlations between Cook-Bolinder, stiffness, values and the face knot area, $CB-TKARF$, smooth face knot area, $CB-TKARSF$, projected knot area, $CB-TKAR$, and smooth projected knot area, $CB-TKARS$, respectively for the 15 beams are shown in Table 1 below.

Table 1: Correlation coefficients for 15 beams when correlating the different knot measures to the Cook-Bolinder stiffness values

Case	Beam	$CB-TKARF$	$CB-TKARSF$	$CB-TKAR$	$CB-TKARS$
144	2	-0.0159	0.0674	-0.1033	-0.1164
146	1	0.3024	0.5040	0.4110	0.6562
147	1	0.0524	0.0760	-0.0327	-0.0400
148	1	-0.1777	-0.2362	-0.2412	-0.4558
149	2	-0.1904	-0.1004	-0.3033	-0.2700
150	2	-0.1396	-0.2934	-0.4341	-0.6652
179	3	0.1114	0.0908	-0.3751	-0.6059
358	1	-0.3236	-0.5049	-0.3972	-0.6978
360	1	-0.1724	-0.2573	-0.3333	-0.4959
363	1	-0.3811	-0.5456	-0.5145	-0.8138
364	1	-0.2062	-0.1626	-0.5299	-0.6354
365	2	-0.2145	-0.3499	-0.3570	-0.6557
369	1	-0.1572	-0.2806	-0.0351	-0.0259
370	2	-0.2633	-0.3506	-0.6243	-0.8134
371	2	-0.1065	-0.1693	-0.2907	-0.4488

5 Strength Versus Projection Values

5.1 Specification of the Subject

The aim of this part of the project is to investigate the relation between $TKAR$ and strength values obtained from Servo-hydraulic Universal Proof Loading machine. There are three different $TKAR$ values that we have the possibility to use in this comparison:

1. $TKAR$ of the whole cross-section, which means that the fraction value is 0.5%
2. $TKAR$ of a part of the upper and lower $TKAR$, fraction is chosen to be 0.25%
3. The weighted value of $TKAR$, see Section 5.2.

The strength values are consisting of one value per beam, which means that we have to find one $TKAR$ value that is representable for the whole beam. There are two different ways to find this value:

1. The value of $TKAR$ in the failure point.
2. The mean value of all $TKAR$ in the proof section, with the centre of the beam as initial point. The sensitivity analysis is used to find the best marginal from the centre point.

5.2 The Algorithm for the Weighted Values of $TKAR$

There are different theories that advocate the relation between position and size of the knots and the strength of beams. As mentioned in Section 1.3.2 the knots located near the edges are the most important edgewise bending properties.

The idea in this algorithm has been established by Carl-Johan Johansson [7] and is based on the *Moment of Inertia*, see Section 3.3, for a triangular area. The algorithm is simplified by using the geometrical centroid of the cross-section instead of the centre of gravity of the cross-section. The following steps are included in the algorithm:

1. Set the Origin to the geometrical centroid of the cross-section.

2. The triangular area is calculated using the determinant of the corner positions

$$\mathbf{AT} = det \begin{pmatrix} X_1 & Y_1 & 1 \\ X_2 & Y_2 & 1 \\ X_3 & Y_3 & 1 \end{pmatrix}$$

3. The Moment of Inertia is determined by dividing the triangular area into its three equal parts with the mass of each is concentrated in the centre point of the three components of the triangle [7]:

$$I = \frac{AT}{3}((\frac{X_1 + X_2}{2})^2 + (\frac{X_2 + X_3}{2})^2 + (\frac{X_1 + X_3}{2})^2)$$

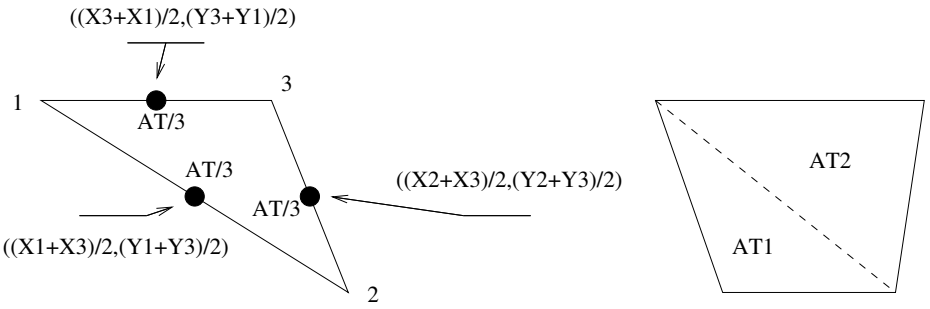

Figure 29: The principle for calculation of the Moment of Inertia of a triangle

According to our assumptions the projected area of a knot is either of trapezoidal or triangular shape. The Moment of Inertia of a trapeze is obtained by summing up the Moment of Inertia of the two triangular parts of the surface, see Figure 29.

6 The Graphical User Interface

One of the aims of this Master's Thesis is to provide a Matlab program with a Graphical User Interface (GUI) to facilitate the usage of the algorithms. The most important purpose of the GUI is that it should enable the user to choose certain values of the variables. Another important purpose of the GUI is that it should enable the user to investigate either one beam or a directory consisting of a group of beams chosen by the user.

The User Interface consists of two different control windows. In the first window the user is able to choose to work with either one beam or a directory containing a group of beams while in the second window the user chooses different variables, and depending on these two, different programs can be run.

The User Interface starts by typing *UI_start*, which is the name of the Matlab program, in the Matlab Command Window. The first window that the user sees is shown in Figure 30.

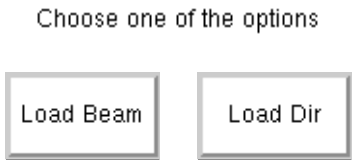

Figure 30: The first window of the GUI with two possible choices

By choosing the *Load Beam* button the second control window pops up, see Figure 31. Here, the user can type variables: *Beam Number*, *Movement Size*, *Window Size*, *Fraction Value*, and also push the *TKARF* button if this information is of interest ($TKAR$ and $TKARS$ is always plotted). The default value of these variables are as mentioned in Section 4.1. The button *CB-START* runs then the program that determines the correlation values between the stiffness values and different knot measures. The output of this program are four different plots: the result of Find-a-partner algorithm, different knot measures together with stiffness values, stiffness values versus $TKAR$ and also $TKARF$ if the user chooses that, stiffness values versus $TKARS$ and also $TKARSF$ if the user chooses that.

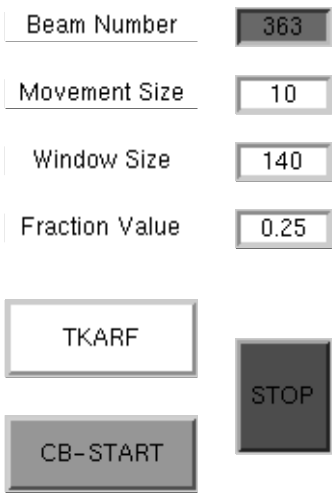

Figure 31: The second window of the GUI if the button *Beam* is chosen

If instead the button *Load Dir* is chosen, the second window pops up as shown in Figure 32. This control window provides the user with the ability to run one of the two programs, either by pushing the button *CB-START*, which runs the program as explained above with the difference that several beams can be run at the same time but no plots are shown, or the button *SU-START*, which runs the program concerning strength values. Pushing *SU-START* results in three plots: the strength values versus $TKAR$, fractional $TKAR$ and weighted $TKAR$.

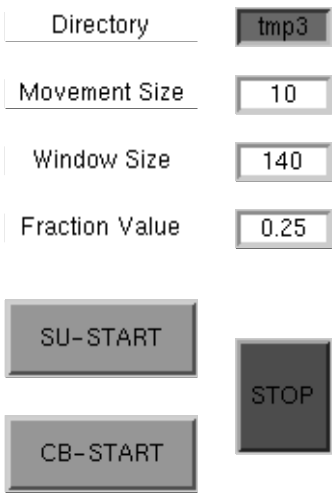

Figure 32: The second window of the GUI if the button *Dir* is chosen

All resulting data and plots from either one of the programs are automatically saved in txt-files during the running of the programs.

7 Results and Discussion

The algorithms are tested for 410 beams, using data from the Soliton Scanning System, the Cook-Bolinder Strength Grading machine and static bending tests. The data have several weaknesses that could depend on the appearance of the beams, for instance weaknesses caused during growth and/or cut process, transportation or storage. On the other side the weaknesses can appear during the testing of the beams in the machines named above. These weaknesses can appear as:

1. The location of the pith can be different on the ends of the same beam. The percentage of such beams is 6%. The main reason for this weakness is that the tree does not grow straight. For those beams the most dominant pith position is then chosen.

2. Dark marks on the flat or edge sides of the beams which appear during the transportation on the outer beams of the package. These marks are detected as knots by the Soliton Scanning System.

3. Splits along the flat sides probably caused during the transportation or storage.

4. Lots of MOE values take form of almost a straight line, which depends on the fact that the mean value is used from the two testings of a beam. This gives small correlations to the $TKAR$, which almost never looks like a straight line. This weakness appears very often and therefor it is disregarded.

With respect to these weaknesses we have chosen to represent the results firstly for all 410 beams and secondly after eliminating 26 defected beams, see point 2 and 3 above.

7.1 Results when Correlating Stiffness Values with Smoothed Total Knot Area Ratio

According to the specification of the project the user is able to choose different sizes of the tested window. We have chosen to illustrate the results using four different window sizes: 100 mm, 120 mm, 140 mm, 160 mm, 180 mm and 200 mm. Our default value for the window is 140 mm which is the basis of our comparisons. The mean value of $CB-TKARS$ correlations

of the 410 beams for the windows named above can be seen in Table 3 below.

Table 2: Mean value of the correlation coefficients of the 410 beams between stiffness values and $TKARS$ for different windows

Window	100	120	140	160	180	200
R	-0.3352	-0.3408	-0.3455	-0.3469	-0.3479	-0.3486

In this project changing the movement size will not be beneficial since we do not have the comparable stiffness values.

After eliminating the defected beams (26 pieces) from the 410 beams the correlation between the stiffness values and the $TKARS$ values for the window size 140 mm became -0.3513, which is a small improvement.

7.1.1 Analysis of the Results

The obtained plots of $TKAR$, $TKARS$ together with the stiffness values and $CWAR$ are used for deep examination of the strong correlations (around 5%), $R \leqslant -0.7$ for $TKARS$, and the weak correlations (around 10%), $R \geqslant 0$ for $TKARS$.

Concerning good results, the MOE curve is rather non-linear and contains several local minima and maxima, which corresponds to high density of knots and low density of knots respectively. An example of such plot can be seen in Figure 33. Another statement is that the knots are equally distributed along the beam and are almost of similar size. Find-a-partner algorithm gives good results concerning the beams with the pith outside, see Figure 34.

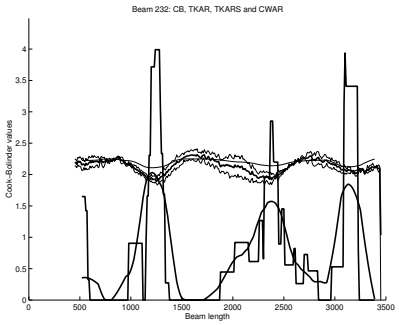

Figure 33: Relation between the Cook-Bolinder values, $TKAR$, $TKARS$ and $CWAR$ for the beam 232. The MOE curve follows the $TKARS$ curve very good.

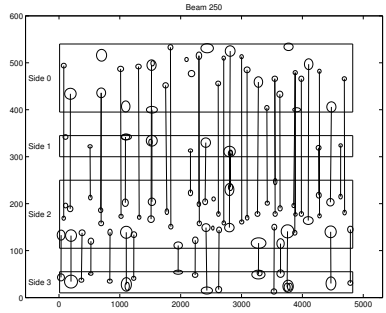

Figure 34: An example of good results from the Find-a-partner algorithm, here for the beam 250.

Concerning bad results, in many cases, the MOE curve is almost a straight line while the $TKARS$ curve consists of local minima and maxima, see Figure 35. If the beam contains another defect, such as compression wood, the MOE curve takes form of a step function, see Figure 36. Find-a-partner algorithm is sometimes the reason behind the bad result. This can be explained by the wrong choice of the in-come side, caused by bad detection, or simply by the limitations of the algorithm, see Section 4.3.1 and Figure 37.

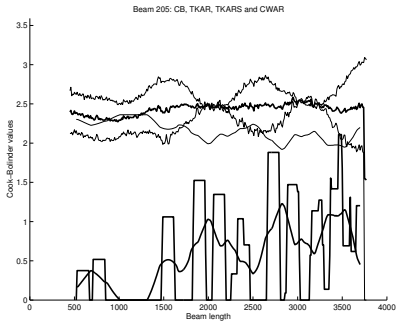

Figure 35: Relation between the Cook-Bolinder values, $TKAR$, $TKARS$ and $CWAR$ for the beam 205. The MOE curve is almost straight while the $TKARS$ curve has several maxima and minima.

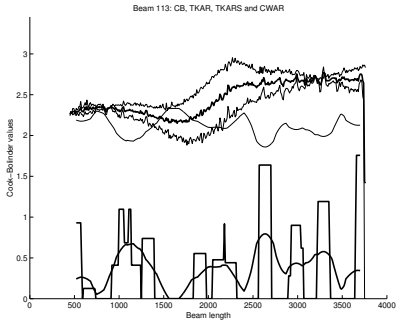

Figure 36: Relation between the Cook-Bolinder values, $TKAR$, $TKARS$ and $CWAR$ for the beam 113. The MOE curve takes form of a step function, due to another defects on the beam.

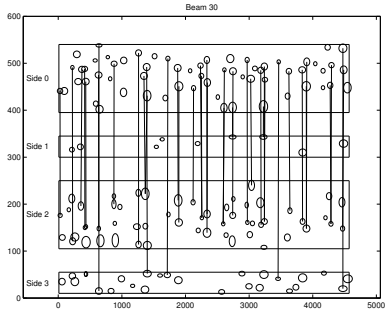

Figure 37: An example of bad results from the Find-a-partner algorithm, here for the beam 30.

7.2 Results when Correlating Strength Values with Total Knot Area Ratio

The aim of this investigation is to find the best coefficient that can explain the strength of a beam. Totally 198 strength values and beams have been used for this purpose. In general the results from the weighted algorithm give the best correlation to the strength. Concerning the unweighted values taking the whole cross-section in account gives better result than taking only a fraction of 25% of it. Other fraction values are not tested within this project but the obtained program gives a possibility for the user to do that.

According to Section 5.1, $TKAR$ in the failure point of the 198 beams is correlated to the strength. In this case the sensitivity analysis is unnecessary because of the fact that the break point is in advance decided in the weakest part of the beam. The results are shown in the tables below together with a few other published results from previous studies which analyze the beams visually [6]. In Figure 38 we can see the plotted values of the strength against the weighted $TKAR$ and the best fitted line to the set of points of 198 beams. The results in the first table show the correlation coefficients for the whole cross-section, $TKAR(50\%)$, the correlation coefficient for the 25% of the both ends of the cross-section, $TKAR(25\%)$, and the correlation coefficient for the weighted $TKAR$ in the whole cross-section, $TKAR(weighted)$. Our result, using our automated method, concerning $TKAR$, see Table 3, is the only comparable value to the presented values from the previous studies shown in Table 4 [6], because the presented values are not weigthed in either way. It is slightly lower, which may depend on several reasons, for instance the detection of the knots and the weaknesses with

our algorithms mentioned previously. We improve the correlation coefficient using the $TKAR(weighted)$ as can be seen in the table. Results in Table 4 consider the relation between $CWAR$ and the strength which explains the positive values.

Table 3: Correlation coefficients for knot measures when correlating with strength values of 198 beams

Knot measure	$TKAR(50\%)$	$TKAR(25\%)$	$TKAR(weighted)$
R	-0.38	-0.34	-0.43

Table 4: Correlation coefficients from previous studies for knot measures when correlating with strength values of beams [6]. These values concern $CWAR$ instead of $TKAR$ and hence the positive values.

Previous study	Isaksson 1	Isaksson 2	Isaksson 3	Johansson
R	0.40	0.34	0.43	0.51

The sensitivity analysis mentioned in the end of Section 5.1 is carried out when correlating the local $TKAR$, the mean value of all $TKAR$ within a prescribed distance on both sides of the centre point of the beam, and the strength with several different distance values. This is illustrated in Figure 39 below. Only the weighted $TKAR$ values are presented. As it is shown in the figure the result gets better as the distance around the centre point of the beam is larger, with the best correlation coefficient -0.4210. This investigation shows that the knots are equally distributed along the beam. The method could be developed to a mathematical model to predict the strength of beams using linear regression.

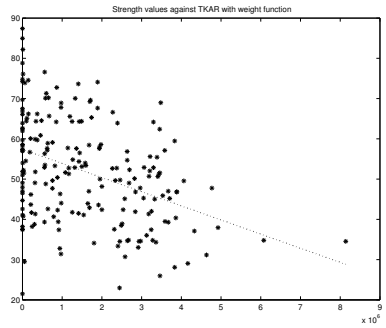

Figure 38: The strength values against the weighted $TKAR$ and the best fitted line

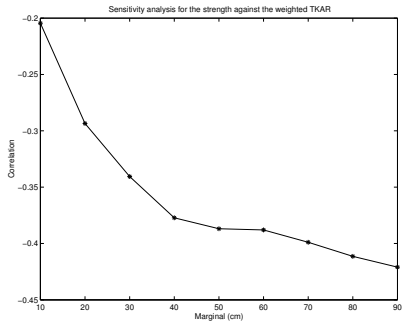

Figure 39: The sensitivity analysis, explained above, for the strength against the weighted $TKAR$

8 Two Common Points of Discussion

8.1 The Symmetry of a Beam

As we mentioned in Section 1.1 there are two common objections concerning the edgewise bending. In this section we investigate the symmetry of beams, in other words, investigate if there are big differences between $TKARU$ and $TKARL$. This investigation can be of big importance when testing the beams in edgewise direction. If the beam appears to be rather symmetric, the bending test can be determined in either of the directions.

A possible way in doing this investigation is outlined in the algorithm below:

1. Determine the key-value, K, for each beam, i, as following:

$$K_i = \frac{TKARU_{max}(i)}{TKARL_{max}(i)}$$

2. Plot the histogram of all K_i

3. Describe the histogram with a suitable distribution

Results

Implementing the algorithm above gives us an assumption that the beams can be concerned as symetric regarding the $TKARU$ and the $TKARL$. The results are shown in Figure 40 containing the histogram, explained above. The distribution of the histogram appears as a normal distribution with mean value 1 and variance 2, $N(1, \sqrt{2})$.

8.2 Reliability of the Tests

In this section we investigate the reliability of the static bending tests in general. As already mentioned, the tests do not include the whole beam length, see Figure 11. For construction wood, this is of relevance when deciding that the tested knot is the weakest area of the whole beam.

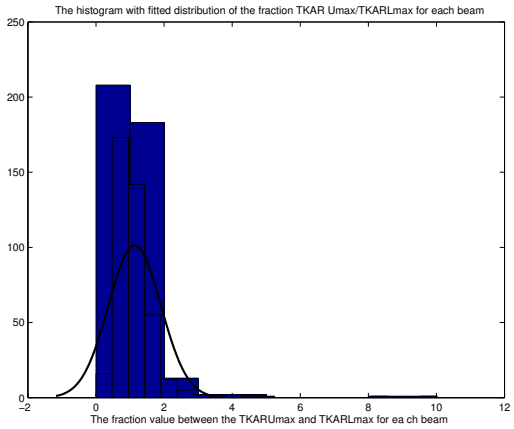

Figure 40: The histogram and the distribution of the differences between the $TKARU$ and the $TKARL$ for 410 beams.

The algorithm below describes this investigation:

1. Find the $TKAR_{max-proof}$ of the proof section, $TKAR_{max}(i)$, for each beam, i,
2. Find the max $TKAR$, $TKAR_{max-beam}(i)$, for each beam, i,
3. If $TKAR_{max-proof}(i) = TKAR_{max-beam}(i)$ count 1, otherwise count 0
4. Determine the fraction of the right tested beams

The proof section of the beam is the whole beam except the distance of $6h+h/2$ from both ends, see Section 2.5, which is 942.5 mm. The result given from the algorithm, by using the distance of 950 mm, is 43%, which means that 43% of all tested beams have the weakest knot in the proof section. We have also determined the mean variance between the $TKAR_{max-proof}$ and the $TKAR_{max-beam}$ which turned out to be 8 percentage points. This value is compared to the maximum value of the $TKAR_{max-proof}$ and the $TKAR_{max-beam}$ to get an idea about how large part of the maximum value it represents. The comparison value turned out to be 16%, which means that this investigation is realistic.

9 Future Work

Currently, there is a Licentiate thesis going on, at Swedish National Testing and Research Institute in Borås and Växjö University, by MSc Rune Ziethen. The subject of Ziethen's Lic. thesis is *Proof Loading - a New Principle for Machine Strength Grading of Timber*. Our master's thesis, mostly the data obtained by the projection algorithms, will be useful for Ziethen when obtaining the mathematical models for his research, which is based on the reliability theory.

During this master's thesis we have established a fact, as many previous studies, that the information about the knots can be used for better understanding of the quality of wood. The difference between this master's thesis and previous studies is that this project uses data from images which are developed in an automatical way, in this case by the Soliton Scanning System. This project provides a good possibility for future work in developing an automatic grading system of beams.

A natural continuation would be, using the computed data in this project, to find a mathematical model for the relation between knots and strength and afterward create an automatical grading system. There is also a possibility to combine different outputs, for instance density or other defects, from the scanning system when creating this kind of grading system.

Another point of view could be to attach importance to the image analysis and predict the position of the pith. This is to a great extent an examination of the fibre patterns. In this project the pith is determined visually and predefined in a text-file.

Appendix A

The images which belong to the beams 363, 364, 370 and 179 are included in this section.

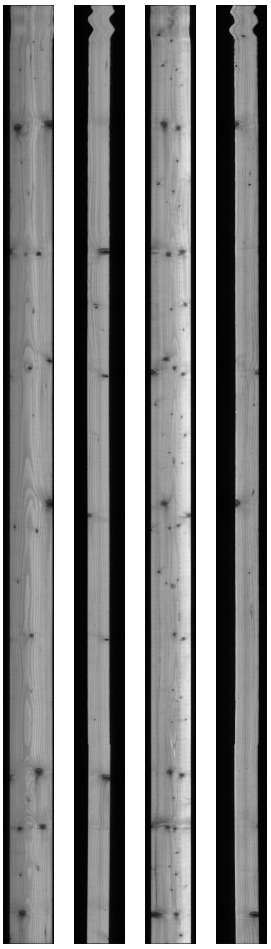

Figure 41: Images of the beam 363 from the Soliton Scanning System

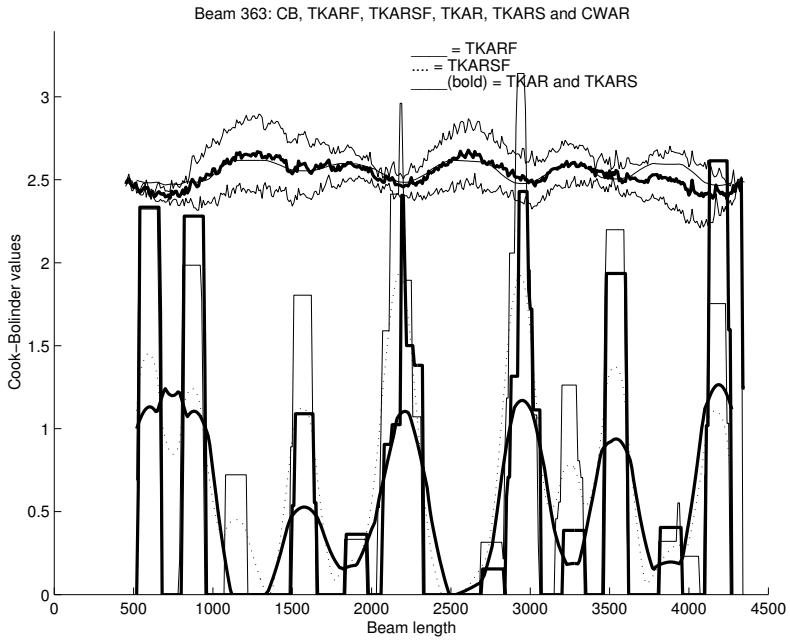

Figure 42: Relation between the Cook-Bolinder values, $TKARF$, $TKARSF$, $TKAR$, $TKARS$ and $CWAR$ for the beam 363.

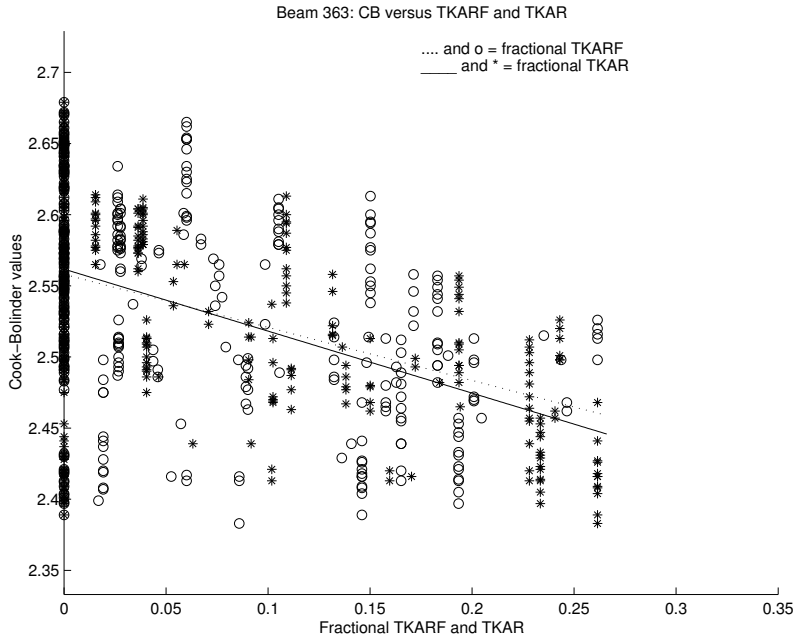

Figure 43: Stiffness values against $TKARF$ and $TKAR$ for the beam 363.

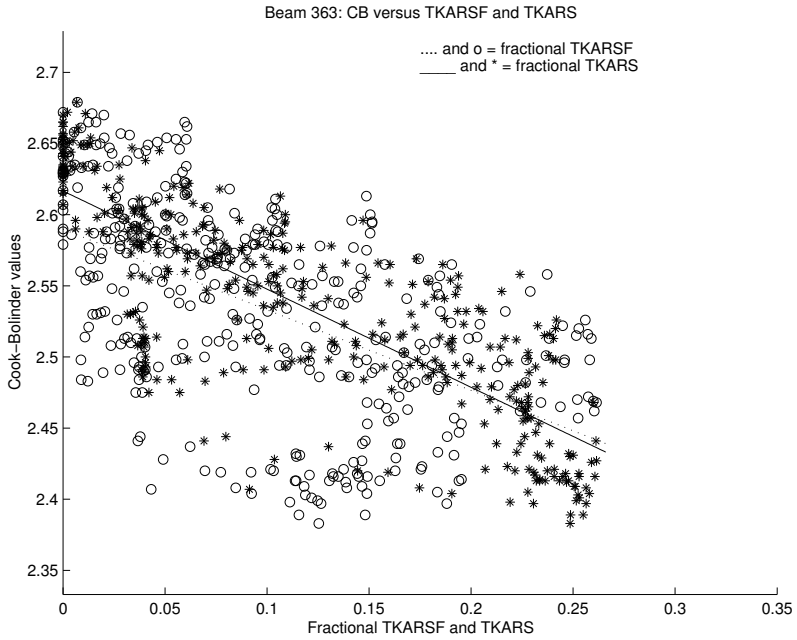

Figure 44: Stiffness against $TKARSF$ and $TKARS$ for the beam 363.

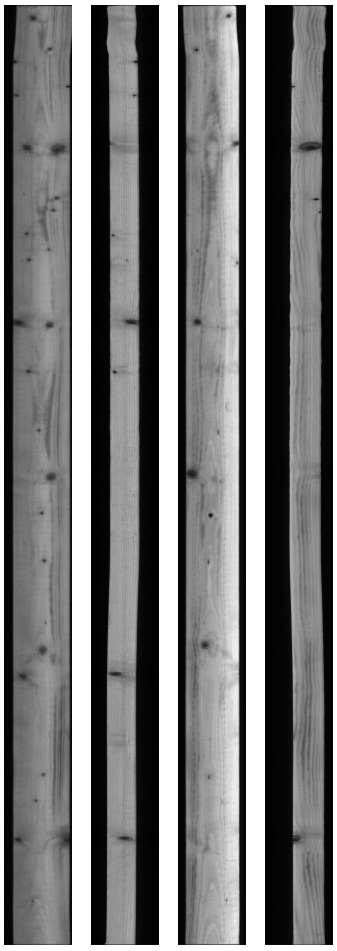

Figure 45: Images of the beam 364 from the Soliton Scanning System

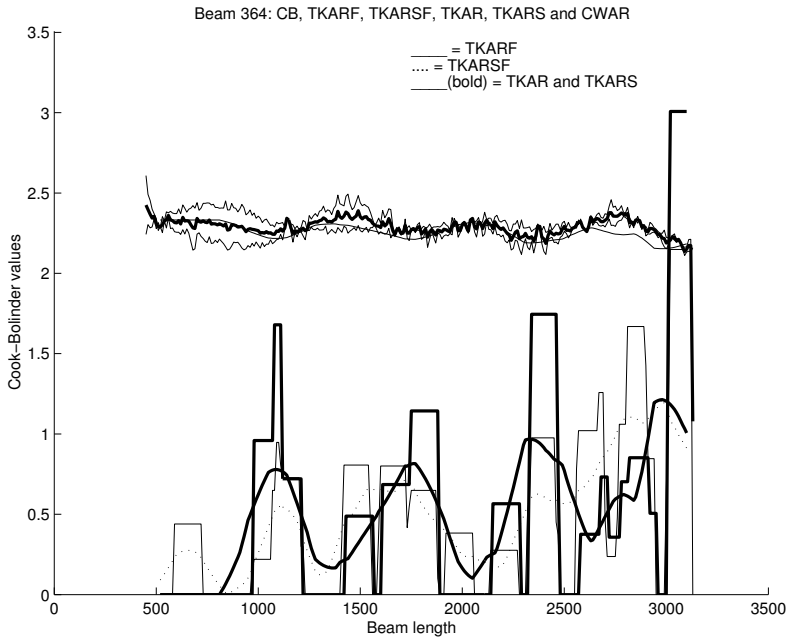

Figure 46: Relation between the Cook-Bolinder values, $TKARF$, $TKARSF$, $TKAR$, $TKARS$ and $CWAR$ for the beam 364.

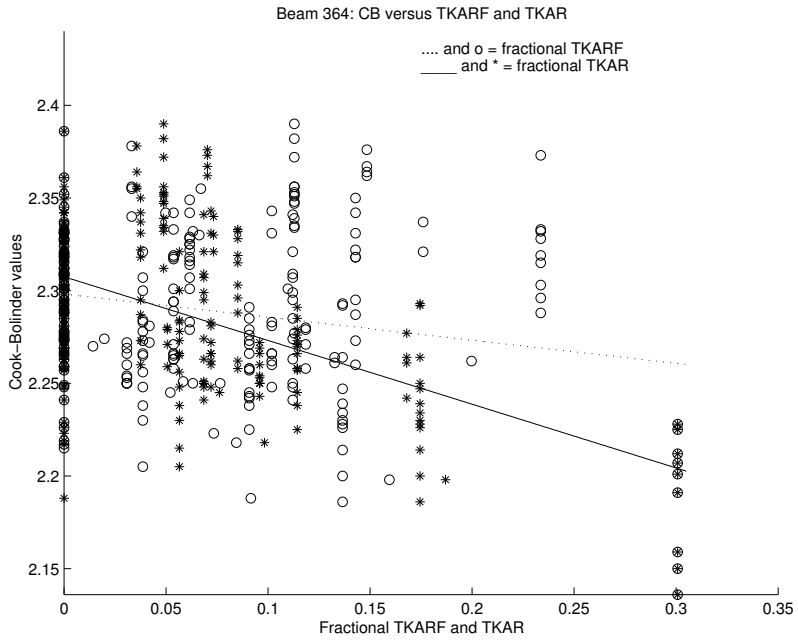

Figure 47: Stiffness values against $TKARF$ and $TKAR$ for the beam 364.

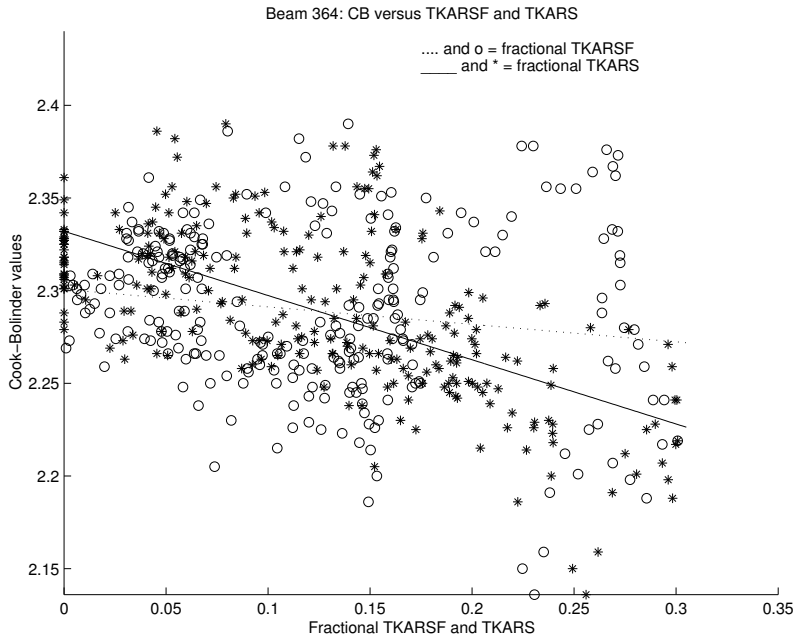

Figure 48: Stiffness against $TKARSF$ and $TKARS$ for the beam 364.

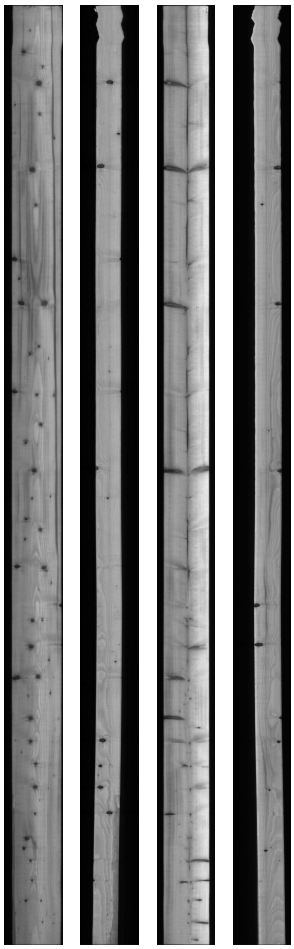

Figure 49: Images of the beam 370 from the Soliton Scanning System

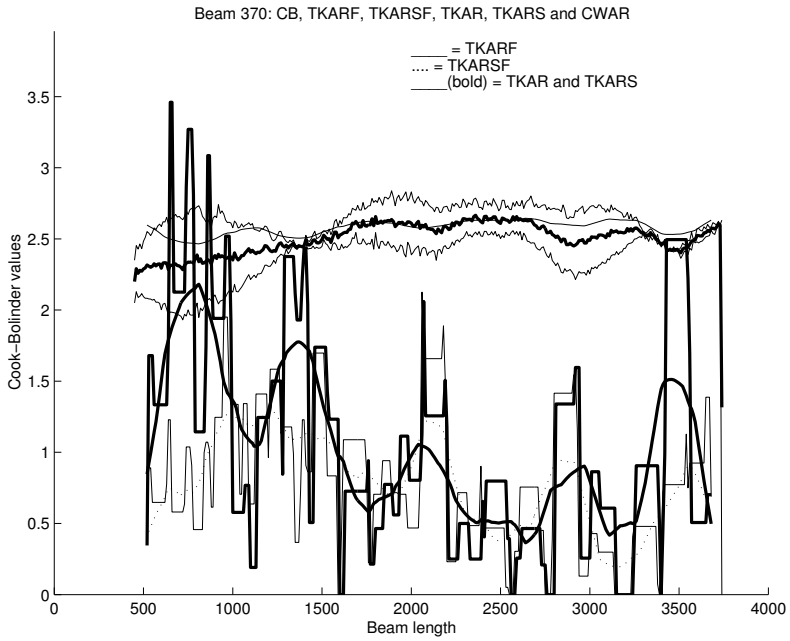

Figure 50: Relation between the Cook-Bolinder values, $TKARF$, $TKARSF$, $TKAR$, $TKARS$ and $CWAR$ for the beam 370, the pith is on the flat side.

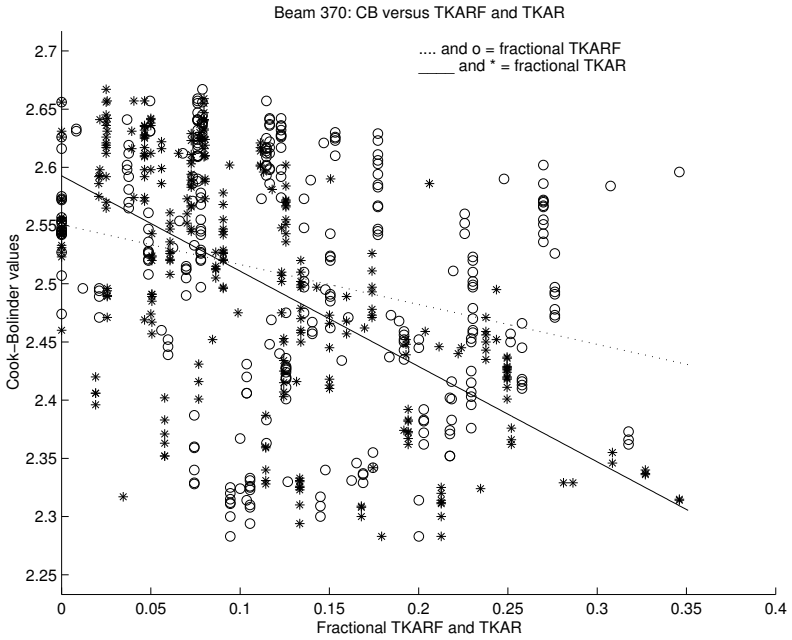

Figure 51: Stiffness values against the knot area and the projected knot area for the beam 370.

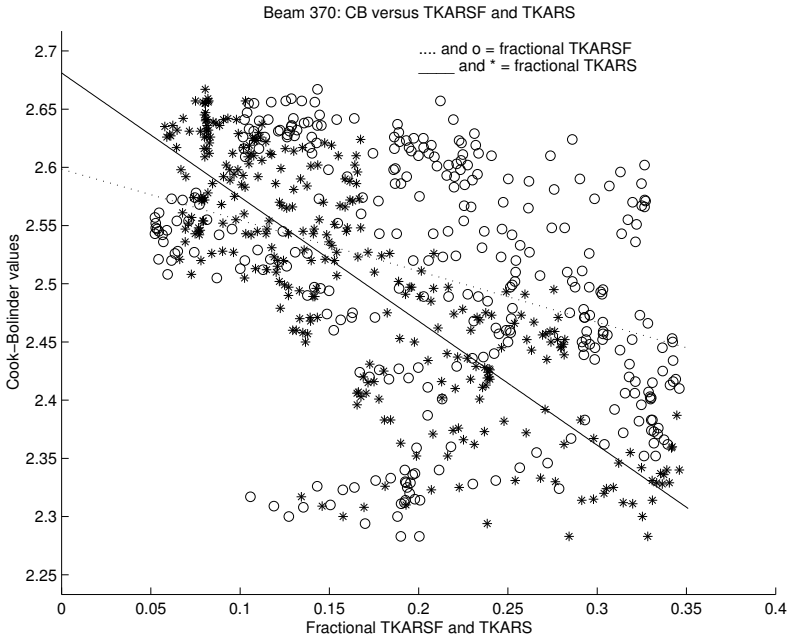

Figure 52: Stiffness against the smoothed knot area and the smoothed projected knot area for the beam 370.

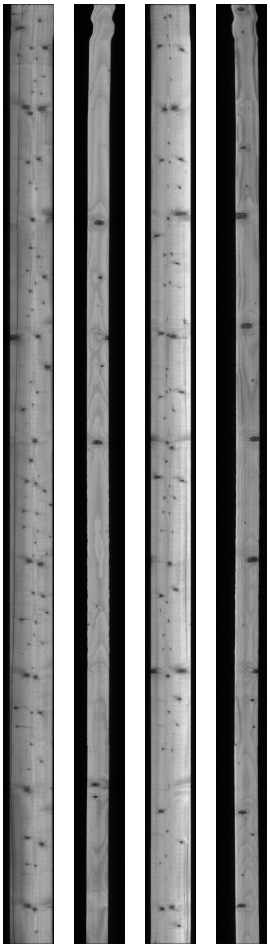

Figure 53: Images of the beam 179 from the Soliton Scanning System

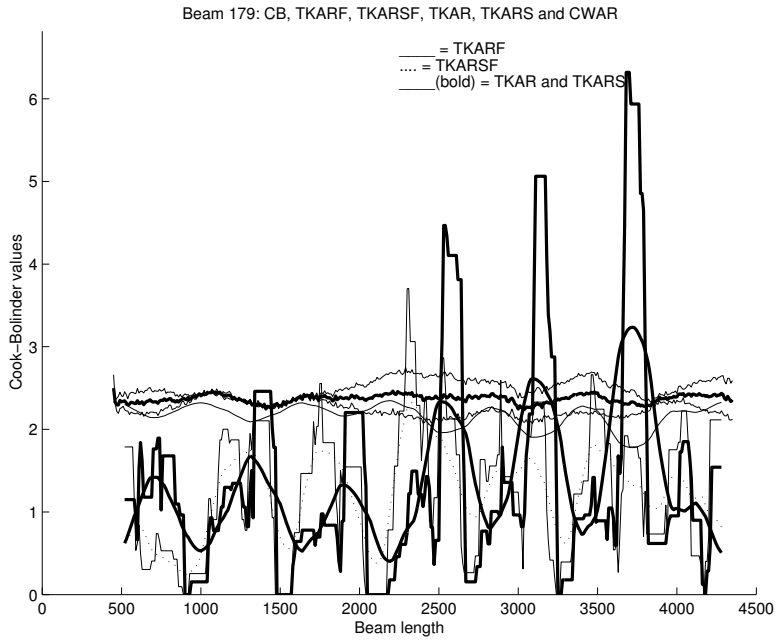

Figure 54: Relation between the Cook-Bolinder values, $TKARF$, $TKARSF$, $TKAR$, $TKARS$ and $CWAR$ for the beam 179, the pith is inside the beam.

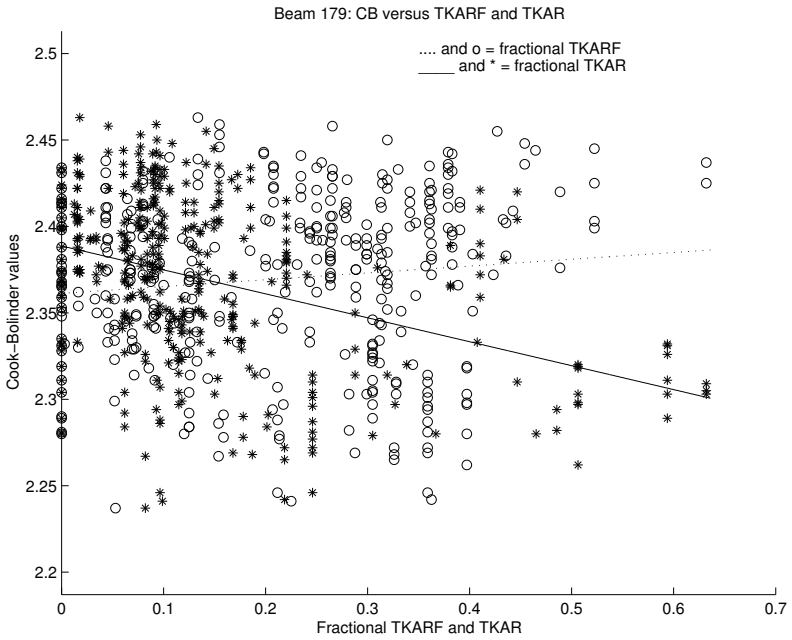

Figure 55: Stiffness values against $TKARF$ and $TKAR$ for the beam 179.

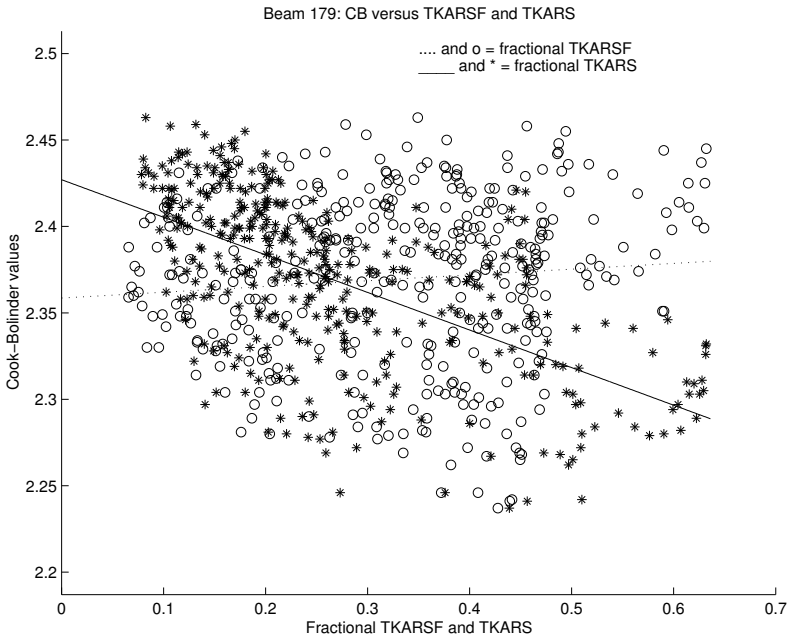

Figure 56: Stiffness against $TKARSF$ and $TKARS$for the beam 179.

Appendix B

The Manual for the Matlab Program

Input Data Files

All input files to the Matlab program are of the data type *.txt* except one which a Matlab file of type *.m*. These text files are then translated by Matlab to matrices, which means that the text files can not contain characters or commas (,). Instead of comma a dot (.) is used for decimals. The names of all input data files are used in the Matlab program, hence all names have to be the same when making new files. Below follows all input data files with corresponding information:

1. **Data**: The input files containing the information about the knots given from a scanning system for a certain beam.
   (a) **Name**: The name of these files contains four symbols, which are the numbers of the beams, and the suffix *.txt*. The names should look as follows:
      i. 0001.*txt*, 0002.*txt*, ... for beams having the number $1-9$
      ii. 0010.*txt*, 0011.*txt*, ... for beams having the number $10-99$
      iii. 0100.*txt*, 0101.*txt*, ... for beams having the number $100-999$
   (b) **Contents**: The data files contain 8 columns with the following contents:
      i. The first column is the number of the beam side (the number of the camera) there the knot is located,
      Soliton A = side 0 (flat side)
      Soliton B = side 1 (edge side)
      Soliton C = side 2 (flat side)
      Soliton D = side 3 (edge side)
      ii. The second column is the position of the knot with respect to the y-axis (the height for flat sides and width for edge sides)
      iii. The third column is the position of the knot with respect to the x-axis (the length of the beam)
      iv. The forth column is the width of the knot (with respect to the x-axis)
      v. The fifth column is the height of the knot (with respect to the y-axis)
      vi. The sixth column is the area of the knot

vii. The seventh column is the diameter of the knot. If this value is omitted, it has to be set to zero.

viii. The eight column is the length of the beam, this value has to be repeated through the whole column.

2. **CB-values**: The data input containing the Cook-Bolinder values.

   (a) **Name**: The name of this kind of data input consists of 5 symbols and the suffix *.txt*. The names should look as follows:

      i. $cb001.txt$, $cb002.txt$, ... for beams having the number $1-9$

      ii. $cb010.txt$, $cb011.txt$, ... for beams having the number $10-99$

      iii. $cb100.txt$, $cb101.txt$, ... for beams having the number $100-999$

   (b) **Contents**: The CB-values contains all data determined by the Cook-Bolinder Strength Grading machine except that commas are replaced by dots and the text above the values is deleted.

3. **SU-values**: The data input containing the strength values together with the positions of the failure point for each beam.

   (a) **Name**: The name of this data file is $brott_values.txt$.

   (b) **Contents**: The file consists of three columns:

      i. The first column is the number of the beam

      ii. The second column is the strength value.

      iii. The third column is the position of the failure point.

   The numbers of the beams do not need to be in specific order, but if a value from the second or the third column is omitted of any reason the whole row needs to be eliminated.

4. **Pith Positions**: This file is the only Matlab file.

   (a) **Name**: This data file is a Matlab function called *pithlocation.m*

   (b) **Contents**: The contents of this data file are shown below

```
%1=the pith is outside
%2=the pith is on the flatside
%3=the pith is inside
%index is the input to the function
%location is the output of the function
```

```
function location=pithlocation(index)

pith=zeros(1,450);
pith(1)=1; %beam 1 has the pith outside
pith(2)=2; %beam 2 has the pith on the flatside
pith(3:5)=3; %beams 3, 4 and 5 have the pith inside
    .
    .
    .
location=pith(index);
```

Output Data Files

These data files are saved in the same directory where the Matlab program exists.

The output data files from the Matlab program are text files (*.txt*) as well as plots (*.ps*). The output data files are presented below:

1. **Values Obtained by CB-START**

   (a) **Name**: These data files are saved as following:

      i. $0001_v alues.txt$, $0002_v alues.txt$, ... for beams having the number $1-9$

      ii. $0010_v alues.txt$, $0011_v alues.txt$, ... for beams having the number $10-99$

      iii. $0100_v alues.txt$, $0101_v alues.txt$, ... for beams having the number $100-999$

   (b) **Contents**: The contents of these files are:

      i. The first column contains the index along the beam for each centimeter.

      ii. The second column contains the Cook-Bolinder values corresponding to the indexes above.

      iii. The third column contains the $TKARU$ values for the corresponding indexes.

      iv. The fourth column contains the $TKARL$ values for the corresponding indexes.

      v. The fifth column contains the $fractional - TKARU$ values for the corresponding indexes.

vi. The sixth column contains the $fractional - TKARL$ values for the corresponding indexes.

vii. The seventh column contains the $weighted - TKAR$ values for the corresponding indexes.

viii. The eigth column contains the $smoothed - TKAR$ values for the corresponding indexes.

2. **Correlations Obtained by CB-START**

   (a) **Name**: This data file is saved as $correlation_CB.txt$.

   (b) **Contents**: The contents of this data file are:

      i. The first column contains the beam numbers.

      ii. The second column contains the positions of the pith.

      iii. The third column contains the correlations $CB - TKARF$.

      iv. The fourth column contains the correlations $CB - TKARSF$.

      v. The fifth column contains the correlations $CB - TKAR$.

      vi. The sixth column contains the correlations$CB - TKARS$.

3. **Plots Obtained by CB-START**

   (a) **Name**: Four different plots are saved, we illustrate the names of these plots for beam number 10 (for example) below, other beams are saved analogically:

      i. The first plot is saved as $beam_10.ps$

      ii. The second plot is saved as $10_fig1.ps$

      iii. The third plot is saved as $10_fig2.ps$

      iv. The fourth plot is saved as $10_fig3.ps$

   (b) **Contents**: See Section 6.

4. **Values Obtained by SU-START**

   (a) **Name**: These data files are saved to $break_values.txt$:

   (b) **Contents**: The contents of this data file are listed below:

      i. The first column contains $TKAR$ in the failure point.

      ii. The second column contains $fractional - TKAR$ in the failure point.

      iii. The third column contains $weighted - TKAR$ in the failure point.

iv. The fourth column contains strength values for the beams.

5. **Correlations Obtained by SU-START**

   (a) **Name**: This data file is saved as $correlations U.txt$.

   (b) **Contents**: The contents of this data file are:

      i. The first column contains the correlations between strength and $TKAR$.

      ii. The second column contains the correlations between strength and $fractional - TKAR$.

      iii. The third column contains the correlations between strength and $weighted - TKAR$.

10 Literature

(a) Åstrand E, *Automatic Inspection of Sawn Wood*, Ph. D. Thesis, Linköping University, 1996

(b) Åström A, *Smart Image Sensors*, Ph. D. Thesis, Linköping University, 1993

(c) Beer F P, Johnston Jr E R, *Vector Mechanics for Engineers, Statics, 6:th edition*, Lehigh University, University of Connecticut, 1996

(d) Boström L, *1st Rilem Symposium on Timber Engineering*, Swedish National Testing and Research, 1999

(e) Glasbey C A, Horgan G W, *Image Analysis for the Biological Sciences*, University of Edinburgh, 1995

(f) Isaksson T, *Modelling the Variability of Bending Strength in Structural Timber, Length and Load Configuration Effects*, Ph. D. Thesis, Lund University, 1999

(g) Johansson C-J, *Draghållfasthet hos limträlameller, Kvistars inverkan på draghållfastheten parallellt med fibrerna hos limträlameller av granvirke*, Chalmers Tekniska Högskola, 1976

(h) Johansson C-J, *Grading of Timber with Respect to Mechanical Properties*, Växjö University and Swedish National Testing and Research Institute, 2002

(i) Kollmann F P, Cote W A Jr, *Principles of Wood Science and Technology, I, Solid Wood*, University of Munchen, State University of New York, 1968

(j) Milton J S, Arnald J C, *Introduction to Probability and Statistics, 3:d edition*, Rodford University, Virginia Polytechnic Institute and State University, 1995

(k) Nyström J,*Automatic Measurement of Compression Wood and Spiral Grain for the prediction of Distortion in Sawn Wood Products*, Ph. D. Thesis, Luleå University of Technology, 2002

(l) Rudemo M, Månsson M, *Random patterns of non-overlapping convex grains*, Advances in Applied Probability vol 34, 2002

(m) Saarman E, *Träkunskap*, Sveriges skogsindustriförbund, 1992

(n) Sonka M, Hlavac V, Boyle R, *Image Processing, Analysis, and Machine Vision, 2:nd edition*, The University of Iowa, Czech Technical University, University of Leeds, 1999

(o) *Timber Structures - Structural Timber and Glued Laminated Timber - Determination of some Physical and Mechanical Properties*, European Standard Ref. No. prEN 408:1994 E, European Committee for Standardization, Brussels, 1994

(p) *Study of the Relationship Between Flatwise and Edgewise Moduli of Elasticity of Sawn Timber as a Means to Improve Mechanical Strength Grading*, Holz Als Roh-Und Werkstoff vol 55, p245-p253, 1997

(q) www.soliton.se